CHALMERS
UNIVERSITY OF TECHNOLOGY

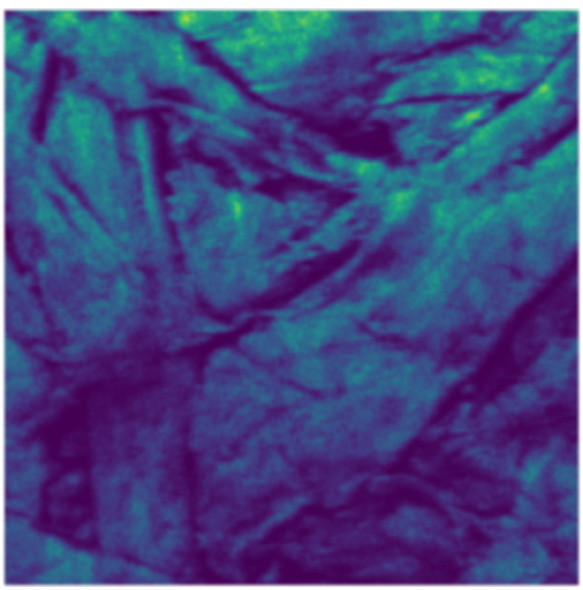
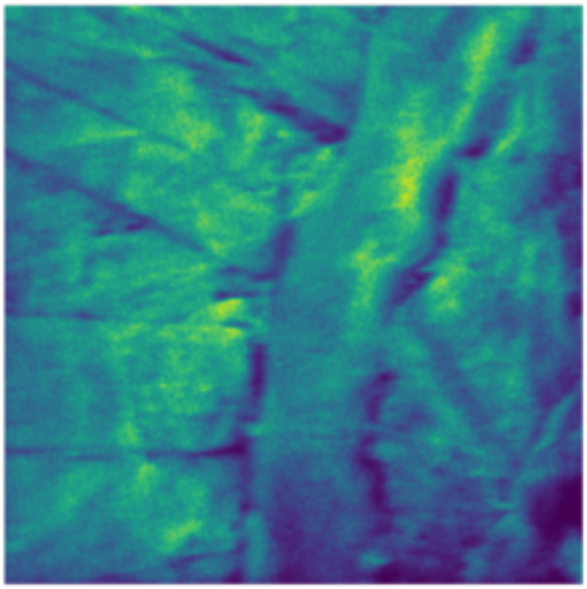

Visualization of Fibre Products Using ToF-SIMS and Multivariate Data Analysis

Master's thesis in Innovative and Sustainable Chemical Engineering

JUTIMA LEKSUNTRAKORN

DEPARTMENT OF CHEMISTRY AND CHEMICAL ENGINEERING
CHALMERS UNIVERSITY OF TECHNOLOGY
Gothenburg, Sweden 2021
www.chalmers.se

Master's thesis 2021

Visualization of Fibre Products Using ToF-SIMS and Multivariate Data Analysis

JUTIMA LEKSUNTRAKORN

CHALMERS
UNIVERSITY OF TECHNOLOGY

Department of Chemistry and Chemical Engineering
Division of Applied Chemistry
Chalmers University of Technology
Gothenburg, Sweden 2021

Visualization of Fibre Products Using ToF-SIMS and Multivariate Data Analysis
JUTIMA LEKSUNTRAKORN

Supervisor: Anette Larsson, Tiina Nypelö, Chemistry and Chemical Engineering
Examiner: Anette Larsson, Chemistry and Chemical Engineering

Master's Thesis 2021
Department of Chemistry and Chemical Engineering
Division of Applied Chemistry

Chalmers University of Technology
SE-412 96 Gothenburg
Telephone +46 31 772 1000

Cover: ToF-SIMS imaging of front side (left) and back side (right) of calendered paper processed at 200℃.

Typeset in LaTeX
Printed by Chalmers Reproservice
Gothenburg, Sweden 2021

Acknowledgements

I would like to express my deep and sincere gratitude to my supervisor and examiner **Anette Larsson** as well as my supervisor **Tiina Nypelö** for giving me the opportunity to do this thesis and providing invaluable guidance, support, and encouragement throughout the process. It was a great privilege and honor to work and study under their guidance. I would also like to thank them for their friendship, empathy, and great sense of humor that have made working with this thesis a much more enjoyable experience. I could not have imagined having a better supervisor and mentor for my thesis.

Besides my supervisors, I would like to thank PhD students, **Roujin Ghaffari** and **Chonnipa Palasingh**, and members of the division whose names may not all be enumerated, for continuous advice and help both personally and on this thesis.

A big thank you to senior researcher, **Per Malmberg**, for assisting me with the ToF-SIMS analysis and to **Mats Josefson** from AstraZeneca for the tutorial session on SIMCA.

The completion of this thesis could not have been accomplished without the collaboration with **Stora Enso, Karlstad Research Center** which provided materials in form of calendered papers and paper sheets .

I am thankful for Stora Enso representative, **Anders Brolin**, for his helpful suggestions and discussions which have lead me to the right direction in my thesis.

To my beloved family, thank you for your love and constant support both emotionally and financially, I am forever grateful. To others who in one way or another shared their support, both emotionally and physically, thank you.

Most of all, I would like to thank God for giving His endless blessings and strength all my life, I would not have accomplished any of this nor be where I am today without you.

Jutima Leksuntrakorn, Gothenburg, August 2021

Visualization of Fibre Products Using ToF-SIMS and Multivariate Data Analysis

JUTIMA LEKSUNTRAKORN
Department of Chemistry and Chemical Engineering
Division of Applied Chemistry
Chalmers University of Technology

Abstract

Physical and chemical complexity of paper and fibre products, makes their spatial analysis challenging. In this study, the visualization of calendered papers was performed using spectroscopic technique, time-of-flight secondary ion mass spectrometry (ToF-SIMS), along with multivariate data analysis (MVDA) to resolve the chemical hierarchy. The chemical difference between the papers calendered at 100°C and 200°C was investigated by using principal component analysis (PCA) and orthogonal partial least squares discriminant analysis (OPLS-DA). Among the observed differences between each side of the papers, the largest variation occurred in lower-mass region (< m/z 100). Potential chemical changes that take place in the higher-mass range (> m/z 300) could not be observed clearly using ToF-SIMS. The findings of this study are essential in expanding the ToF-SIMS library of paper and paper components, and demonstrates that multivariate analysis methods are needed for resolving the differences in spectral data of hierarchical materials.

Keywords: ToF-SIMS, MVDA, paper composition.

Contents

List of Figures

List of Tables

Abbreviations

AFM - Atomic Force Microscopy

CNC - Cellulose Nanocrystals

CTMP - Chemo-thermomechanical Pulp

DMAC - Dimethylacetamide

DMF - Dimethylformamide

DMSO - Dimethyl Sulfoxide

FTIR - Fourier Transform Infrared Spectroscopy

GGM - Galactoglucomannan

HT-CTMP - High Temperature Chemo-thermomechanical Pulp

MCC - Microcrystalline Cellulose

MVA - Multivariate Analysis

MVDA - Multivariate Data Analysis

OPLS - Orthogonal Partial Least Squares

OPLS-DA - Orthogonal Partial Least Squares Discriminant Analysis

PCA - Principal Component Analysis

PDMS - Polydimethylsiloxane

RMP – Refiner Mechanical Pulp

SIMCA - Soft Independent Modeling of Class Analogy

SSNMR - Solution-state Nuclear Magnetic Resonance Spectroscopy

TMP - Thermomechanical Pulp

ToF-SIMS - Time-of-flight Secondary Ion Mass Spectrometry

1
Introduction

In an earlier study [1], lignin migration, lignin cross-linking, and van der Waal interactions have been subjected to occur during the calendering of paper. Potential other reactions such as lignin-furfural linkages [2] and furfural self-polymerization [3] have also been proposed. Several spectroscopic techniques such as Raman, Fourier transform infrared (FTIR), and high-resolution solution-state nuclear magnetic resonance (SSNMR) spectroscopies have been applied to investigate the morphology and chemical composition on fibre products. However, time-of-flight secondary ion mass spectrometry (ToF-SIMS) comes closest to the ideal technique of chemical microscopy, as both the chemical specificities and the spatial resolution of the distribution of components in lignocellulosic materials can be obtained, yet the literature data about paper and fibre product analysis by ToF-SIMS are very limited.

Therefore, this thesis is conducted by means of ToF-SIMS together with multivariate data analysis method to determine the surface chemical composition and distribution on paper during the calendering with different raw materials of wood components were being analysed as references.

1.1 Objective

The objective of this thesis is to demonstrate the capabilities of spectroscopic visualization technique to determine the chemical composition and distribution of wood components in paper. Experimental work is directed to observe the spatial chemical changes in paper processed at different conditions, analysis of model materials and ToF-SIMS library build up.

1.2 Hypothesis

As one of the main components in paper, lignin is hypothesized to alter during the calendering. A step to achieve better understanding of the composition and distribution of wood components in such paper can be determined by using a combination of spectroscopic technique and multivariate statistical analysis to differentiate and identify the chemical alterations in the material processed at different condition.

2
Background

2.1 Structure of Wood

Wood, as the most common bioresource for storing carbon dioxide, is produced from trees [4]. Each tree can be divided into three main parts, namely, the crown, stem, and root. In general, the stem is considered as the crucial part of the tree for nutrient transportation and storage, mechanical support, growth and protection and is used as the main renewable raw material in pulp and paper industry due to its higher content in cellulose compared to other tree parts. Each wood tissue consists of various wood cell types that have different functions and compositions in the tree. These compositions vary between different climate, season, growth conditions, and tree species such as softwood and hardwood.

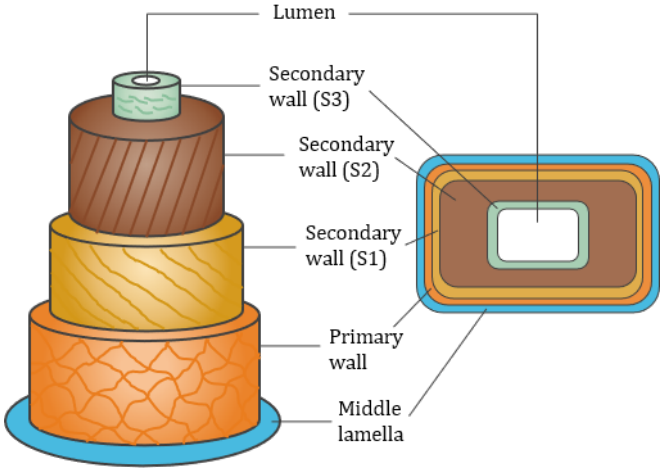

Figure 2.1: Schematic illustration of a typical wood cell wall structure composing of a hollow lumen surrounded by secondary layers (S1, S2, S3), primary layer, and middle lamella.

Wood cells, consist mainly of cellulose, hemicellulose and lignin, are multilayered with the hollow center called lumen which are surrounded by a complex cell wall, as seen in Figure 2.1. These wood cells are binded together by lignin-rich middle lamella (ML) region. The outermost layer next to the middle lamella called the primary cell wall (P) is composed of randomly orientated cellulose microfibrils [4]. The secondary cell wall consists of 2-3 layers known as S1, S2, and S3, having the central S2 layer makes up the major part while S1 and S3 layers are comparatively

thin. In addition, the orientation of cellulose microfibrils, which differs in these layers, is of great importance for the physical properties of the wood cell and thus for the structure of the wood.

Cellulose, one of the main components, makes up about 50% by weight of the wood substances [5]. It is a linear polymeric chain of β-D-glucose monomers, linked together by β-(1-4)-glycosidic bonds (Figure 2.2). These chains organized into bundles called cellulose microfibrils which further aggregated into macrofibrils. Because of its linear structure, cellulose is able to form strong intermolecular interactions within the microfibrils and chains through hydrogen bonding. In addition, the high molecular weight, stiffness, hydrophobicity and the special morphological organizations of cellulose all together makes it resistant to dissolution.

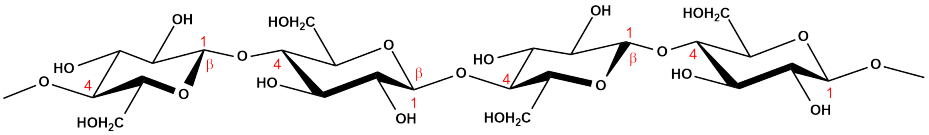

Figure 2.2: Chemical structure of cellulose.

Hemicelluloses are another one of the main constituents of wood, usually around 20 to 35 % of dry mass [4]. They situated in the matrix between cellulose fibrils in the cell wall and are subjected to serve as an interface between cellulose and lignin. They are branched, heteropolysaccharides made up of various types of pentoses (D-xylose and L-arabinose) and hexoses (D-glucose, D-mannose and D-galactose) [4] shown in Figure 2.3. One, two or more types of monomers, connected to each other by β-(1-4)-glycosidic bonds, often form the backbone of hemicellulose polymers. Most hemicelluloses also have short branches that contain different types of sugars and acetyl side groups. They are highly soluble and reactive, therefore easily degraded by chemicals and heat treatment. Two main groups found in wood are xylan and glucomannan, where xylan is the main hemicellulose in hardwoods as glucomannan in softwoods.

Furfural is a valuable product that can be obtained from dehydration reaction of hemicellulose, mostly from C5 sugars i.e. xylose (Figure 2.4). It can be converted into fuels and other useful chemicals used in oil refining, plastics, pharmaceutical, and agrochemical industries [6].

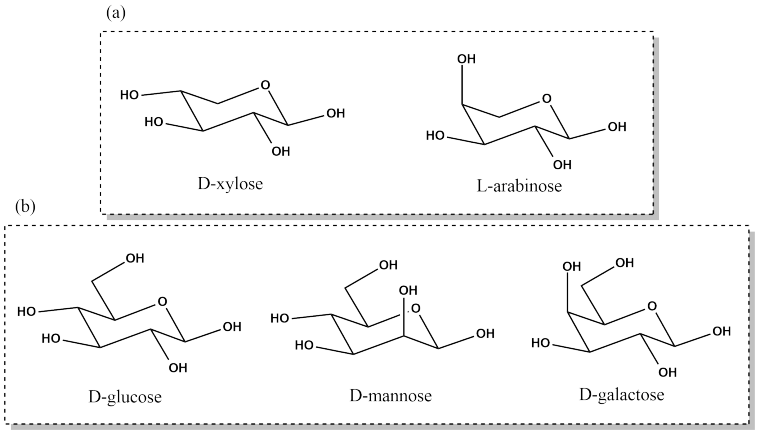

Figure 2.3: Monosaccharide units; (a) Pentoses; D-xylose and L-arabinose , (b) Hexoses; D-glucose, D-mannose, and D-galactose.

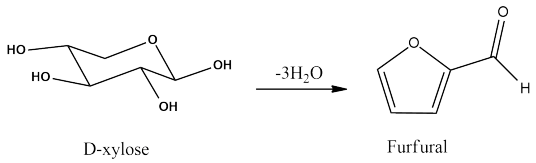

Figure 2.4: Dehydration of hemicellulose to furfural.

Lignin is an extensively branched three-dimensional network which composed predominantly of three monomers known as monolignols [4], that is, p-coumaryl alcohol, coniferyl alcohol, and sinapyl alcohol, as seen in Figure 2.5. Based on these monolignol units, the lignin building blocks p-hydroxyphenyl (H), guaiacyl (G), and syringyl (S) are formed. These building blocks are connected by various types of linkages (Figure 2.6), mainly ether bonds (C-O-C) such as aryl- or diaryl ether and carbon-carbon bonds (C-C) such as biphenyl or pinoresinol, which are distributed randomly.

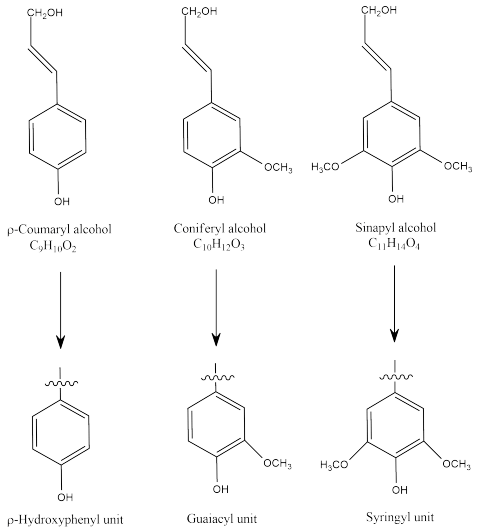

Figure 2.5: Structure of the three monolignol precursors and their corresponding fragments in the macromolecules.

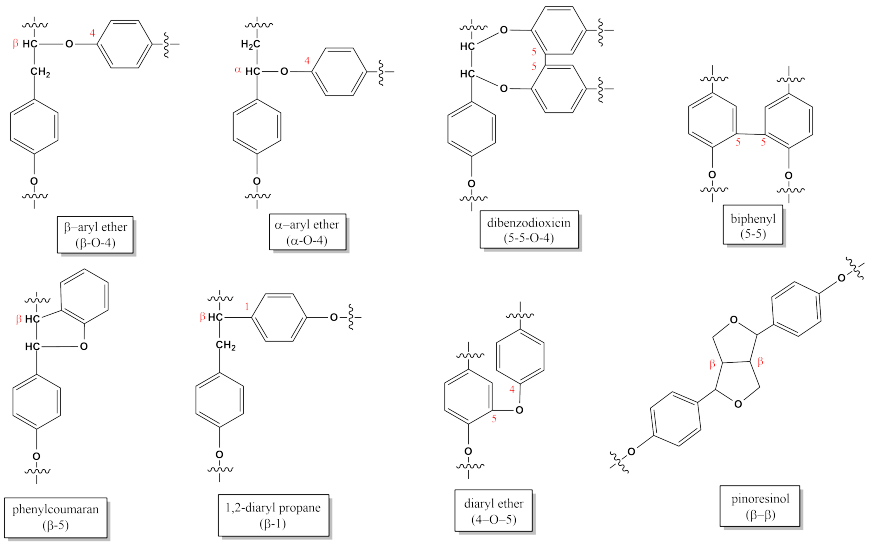

Figure 2.6: Lignin interunit linkages: ether bonds, carbon-carbon bonds, and other linkages.

Lignin macromolecule also consists of different functional groups that affect its reactivity, such as methoxy groups, phenolic hydroxy groups, and a few terminal aldehyde groups [4]. Lignin polymerization reactions, initiated by oxidation of the phenylpropane phenolic hydroxyl groups, result in a complex and highly-branched structure. Therefore, it is difficult to determine lignin chemical composition. The monolignol composition, content, and concentration is varied between wood species. Several hypothetical lignin structures have been presented over the years, with Figure 2.7 showing a suggested model of softwood lignin. However, the most common intermonomeric linkage in lignin is the β-O-4 aryl ether bond [7].

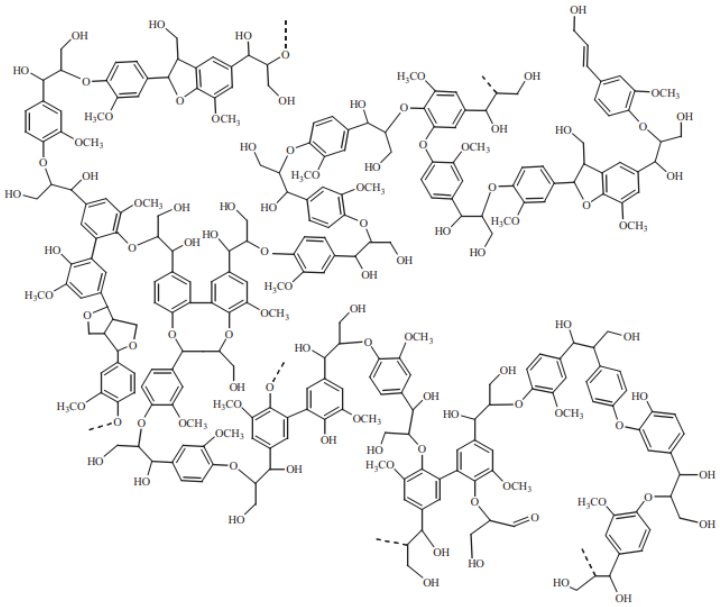

Figure 2.7: A suggested model of softwood lignin. *Reproduced with permission from [4].*

Extractive substances, pectin, and inorganic compounds are also present, even if only as minor components. Wood extractives, situated outside the cell wall, are low molecular weight compounds that can be extracted from the wood with neutral organic solvents or water [8] and are the cause of several paper properties such as the binding between fibres, the water adsorption and friction including the smell of the paper. The majority of these compounds are *aliphatics*, *terpenoids*, and *phenolics*. Aliphatics group includes fatty acids and fatty alcohols, with fatty acids mainly present in ester form, either esterified with glycerol in the form of mono-, di-, and triglycerides (fats) or as esters with fatty alcohols (waxes) or sterols (steryl esters). Within terpenoids group, there are a vast number of different terpenes built up by isoprene units (5 carbons). The remaining phenolics are stilbenes, flavonoids, lignans, tannins, and tropolones. Some of the extractives are shown in Figure 2.8.

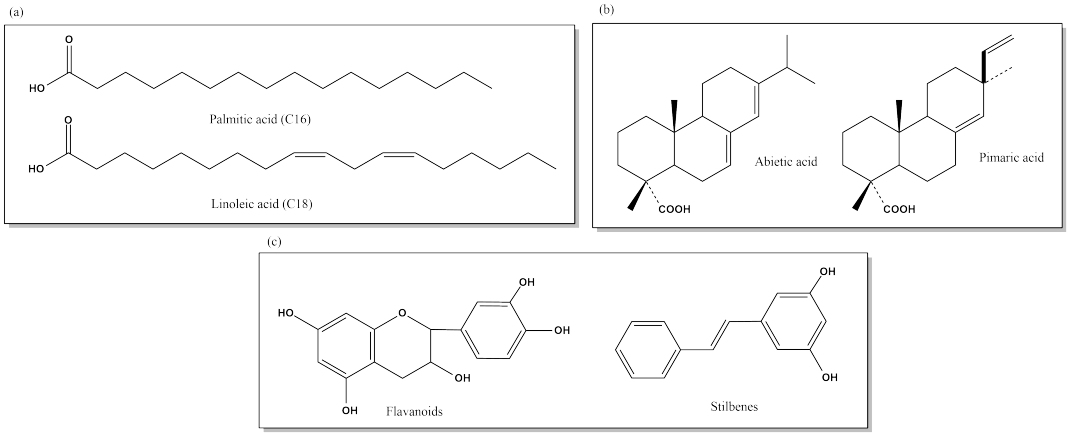

Figure 2.8: Extractive compounds: (a) Aliphatic compounds, (b) Terpenes, and (c) Phenolic compounds.

2.2 Pulping Processes

Pulp consists of fibers that are generally obtained from wood. The pulping processes have the main aim of releasing the fibers from the wood matrix, which can be achieved mainly in two ways, either mechanically or chemically [9].

2.2.1 Mechanical Pulping

When wood or wood chips are grounded, the wood fibres are released and a mechanical pulp is obtained. Some easily soluble carbohydrates and extractives are lost in the process, but the overall pulp yield is hardly affected. The mechanical pulp yield is approximately 90 to almost 100%, depending on the mechanical pulping method used [9]. The fibres are fractionated generally at the middle lamella, primary cell wall or the secondary cell wall, depending on pretreatment of wood chips prior to the grinding. In addition to refining at elevated temperature and pressure, pretreatments aim to soften the lignin and weaken the lignin-rich middle lamella to promote fracturing in this area. The pulp made without preheating of the wood chips with steam called *refiner mechanical pulp* (RMP) tends to have fines and fractures across fibres. *Thermomechanical pulp* (TMP) is made by refining the wood chips at elevated temperature and pressure. In *chemo-thermomechanical pulp* (CTMP) process, a chemical treatment with softening chemicals impregnate the wood chips prior to the refining is followed by a steam pretreatment. Additionally, the *high temperature chemo-thermomechanical pulp* (HT-CTMP) process adds a further pretreatment step in which the wood chips are preheated before refining.

2.2.2 Chemical Pulping

Fibres in wood are glued together by lignin. The chemical method of producing wood pulp is to attack the lignin in middle lamella and thereby, release the individual fibres. By removing lignin from cell wall, the fibres get flexible enough to give high strength to the paper.

Kraft pulping, also known as an alkaline process involves using cooking chemicals composed of sodium hydroxide ($NaOH$) and sodium sulfide (Na_2S), in other words, white liquor. The active chemicals are thus, hydroxide ions (OH^-) and hydrogen sulfide ions (HS^-). The aim of this process is to degrade and dissolve lignin with the main delignification reaction, cleavage of interunit linkages [9]. The process can be divided into four main steps as seen in Figure 2.9, which include steaming as pretreatment, impregnation of wood chips with cooking chemicals, delignification or disintegration and solubilization of lignin with hydrogen sulfide as the major delignifying agent and blowing as the last step to lower the temperature and pressure to stop the chemical reactions. Several stages of bleaching are included as a chemical process aimed at removing colour in the pulp, residual lignin or carbohydrate by-products. During the kraft pulping, the majority of lignin is removed but the pulping chemicals are not completely selective towards lignin and as a result, carbohydrates, especially the hemicelluloses, are also lost to a varying extent which in turn, results

in a low pulp yield, usually around 50% [7].

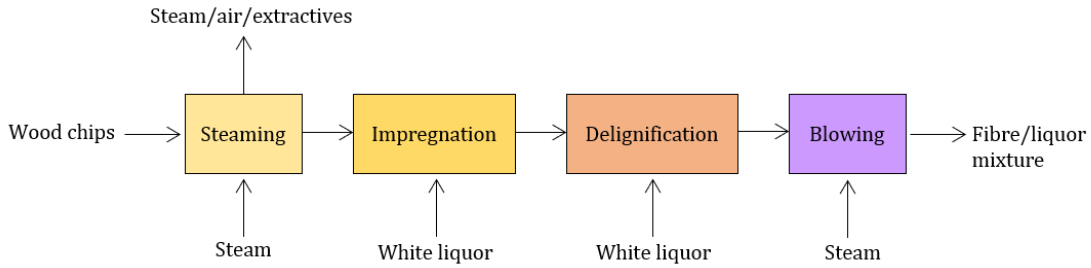

Figure 2.9: Technical steps in kraft pulping process.

There are three phases of delignification during kraft pulping, which are initial phase, bulk phase, and residual or final phase (Figure 2.10). In initial phase, occurring at temperature below 150℃, the dissolution of lignin is approximately 15-20% while the loss of carbohydrates is about 20-25%. Most of the delignification takes place in the bulk phase at the temperature between 150-170℃ whereas carbohydrates remain stable. In the residual phase, the selectivity of lignin is poor, thus the dissolution of lignin is very slow while the degradation of carbohydrates becomes substantial.

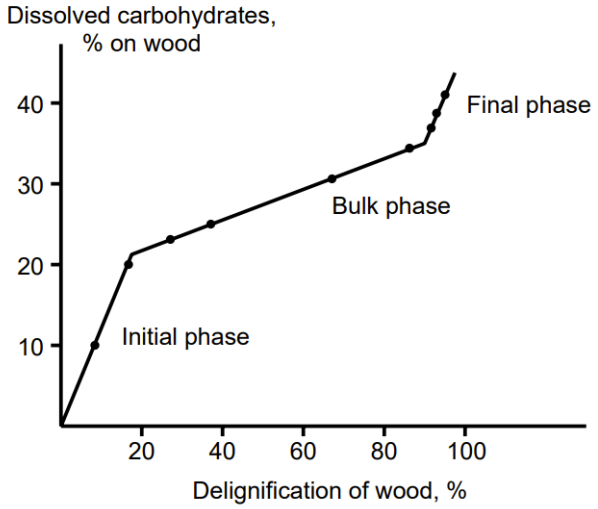

Figure 2.10: The selectivity of delignification in the three phases of kraft pulping. *Reproduced with permission from [10].*

Sulfite pulping is another chemical approach in pulping process where in most cases, an acidic bisulfite proceed is employed to soften the wood materials by removing lignin. The active chemicals used in this process are sulfur dioxide (SO_3^{2-}) and/or hydrogen sulfite or bisulfite ions (HSO_3^-) [11]. Four different bases or cations, that are calcium (Ca^{2+}),magnesium (Mg^{2+}), sodium (Na^+), and ammonium (NH_4^+), can be used to buffer the pulping solution. These ions react with lignin to produce water-soluble sulfonated lignins, so called lignosulfonates. The efficiency of delignification during sulfite pulping depends on both sulfonation and hydrolysis reactions [12]. Sulfonation reaction makes lignin more hydrophobic by introducing sulfonic

groups while hydrolysis reaction breaks the ether bonds and creates new phenolic groups, which in turn increases the hydrophilicity of lignin and reduces its molecular weight. The drawbacks of sulfite pulping compared to kraft pulping, however, are more pollution emitted to the atmosphere, applicable to fewer wood species due to limited abilities to dissolve extractives, lower strength potential of pulp, and poor chemical recovery.

2.3 Paper Manufacturing Process

The papermaking process includes two main processes which are *Wet End Operation* where cleaned and bleached pulp is formed into wet paper sheets and *Dry End Operations* where prior wet sheets are dried and several surface treatments are applied to the paper [13].

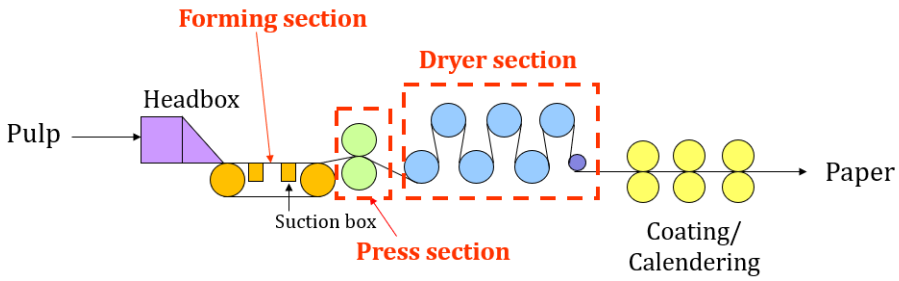

Figure 2.11: Schematic illustration of Fourdrinier Paper Machine

Fourdrinier machine is widely used in papermaking process [13]. It is comprised of three primary sections: the forming section, the press section, and the dryer section, as seen in figure 2.11. Pulp consisting of about 0.5 to 1.0 % fibre is fed or pumped into a headbox where it flows out onto a moving wire belt. The pulp is squeezed through a series of rollers while suction devices below the belt drain off the water which leaves the fibre to form a wet mat of paper. This paper then enters the press section where it is pressed between rolls of wool felt and then passed through a series of steam heated cylinders in the dryer section to remove any remaining water. This resulting in a continuous paper roll or *web* which is generally subjected to various finishing steps before it can be shipped as a final product.

2.3.1 Calendering Process

Calendering is considered as one of the final steps in the paper manufacturing process that aims to improve the surface properties of paper with regards to its further use, e.g., printing. It can make paper surface extra smooth and glossy or even give a more uniform thickness. During calendering, the paper web is compressed between two or more rolls where heat and pressure are applied which can be significantly high (10-50 MPa) during a very short time (less than 1 ms) [14]. The term calendering encompasses a wide range of specialized machines having different names depending

on its position in the production line, in the middle or the end of the machine, online or offline, and depending on the design of the rolls.

The *machine calender*, made of hard rolls or soft rolls (named nip), is located online after the drying section in the paper machine [14]. Its main purpose is to bring surface roughness and gloss of uncoated paper to the desired level. This type of calenders can also be placed prior to the coating unit in order to control the degree of roughness and the thickness profile. The *soft calender* includes one to four nips made from heated steel rolls and polymeric soft rolls. This calender, located at the end of paper machine, is used as the final finishing step to develop the surface properties of both coated and uncoated papers. The *supercalender* and the *multinip calender* are made from six to sixteen nips with the main purpose on producing paper with the highest level of gloss and smoothness. Traditional supercalender is placed off-machine and multinip calender can be either online or offline.

Nevertheless, there is an issue when it comes to the improvement of paper surface properties. The inevitable consequence from applying the pressure between at least two rolls is that the paper thickness is decreased which is not acceptable for some paper grades. To develop gloss without decreasing too much of the thickness, machine glazed calender and gloss calender were used [14]. *Machine glazed calender* is used to develop gloss on one side of the paper. Its principle is to use friction forces between the paper web and a hot cylinder to glaze one side of the paper. This device is usually used in the production of uncoated grade papers. The latter, *gloss calender*, is used to develop gloss on specialty coated grade papers or boards. Its principle is to press one side of the paper against a hot chromium plated roll, usually around 140 to 200℃, while another roll covered with rubber is soft and ensures good contact than applying pressure.

2.3.1.1 Softening of paper

The softening behavior depends on the pulp type [15] and is related to the glass transition temperature of the polymers situated in the fibers.

The glass transition temperature is the thermal transition when a polymer changes from a rigid, glassy, brittle state to a soft, moldable, ductile state [14]. Since fibers consist of cellulose, hemicellulose and lignin, this transition is called the softening temperature of the paper. The glass transition temperature is very difficult to measure in a polymer with a broad size and composition. Therefore, the values reported in the literature vary over a wide range. However, the trend is observed that the glass transition temperature is probably between 230 and 255℃ for cellulose, between 165 and 217℃ for hemicellulose, and between 134 and 235℃ for lignin.

In these polymers, water acts as a plasticizer and therefore lowers the glass transition temperature, as seen in Figure 2.12. The fibers on the paper surface will exceed the glass transition temperature and become easily moldable while the fibers within the paper will remain below the glass transition temperature and as a result, remain rigid.

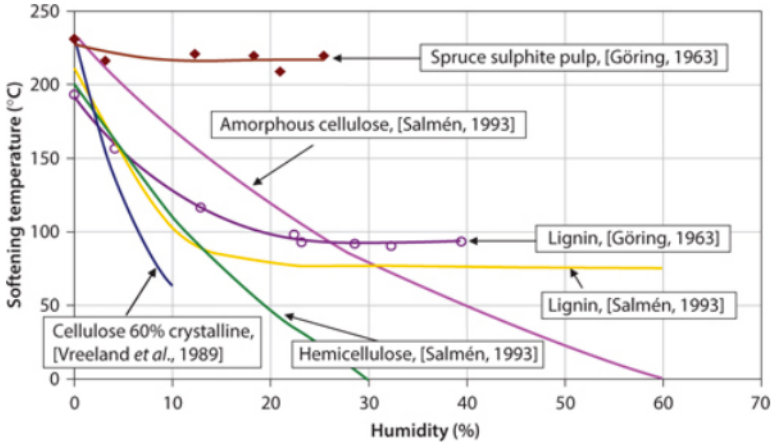

Figure 2.12: Softening temperature of wood components with humidity. *Reproduced with permission from [14]*

2.4 Secondary Ion Mass Spectrometry (SIMS)

SIMS is a mass spectrometry technique involves bombarding a sample surface with an ion beam called *primary ions* and analyzing the ions produced by the bombardment called *secondary ions* [16]. The main principle of SIMS method is the use of a focused ion beam of primary ions, generated by a liquid metal ion gun (LMIG). The energy of the primary ions is transferred to the target atoms through atomic collisions, creating a collision cascade [17]. Primary ions set atoms in motion, both through direct collisions with atoms in the sample and indirectly through collisions between atoms that are already in motion with other target atoms (Figure 2.13). Energy is transferred back to the surface which allows surface atoms and molecules in the top 2-3 molecular layers to exceed their surface binding energy. Although most secondary ions come off neutrally charged, a small part comes off either as positive or negative ions which can be analyzed according to their mass to charge ratio m/z.

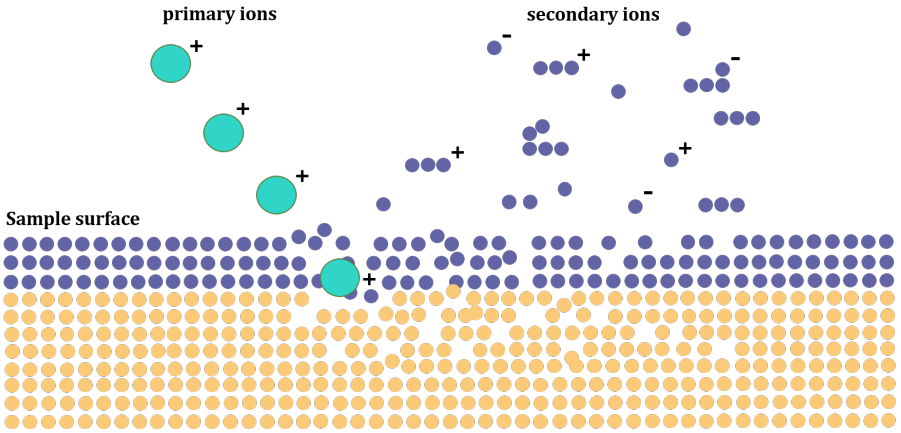

Figure 2.13: Schematic illustration of the secondary ion emission process initiated by the impact of a primary ion.

Depending on the ion dose, the technique can be divided into two modes which are dynamic and static SIMS [17]. As opposed to dynamic SIMS, static SIMS is performed with low primary ion doses. Only about 1% of the surface layer is impacted by the primary ions, yielding chemical and molecular information of the original surface and resulting in sensitive analysis from the uppermost molecular layers with minimized sample damage.

2.4.1 Time-of-Flight Secondary Ion Mass Spectrometry (ToF-SIMS)

ToF-SIMS is a combination of the static SIMS technique and time-of-flight mass analysis (ToF), with the principle based on the fact that ions with different masses travel with different velocities. The measurement is carried out under high-vacuum conditions. ToF-SIMS is a powerful technique that provides direct analysis of chemical information on the surface of a solid sample without a chemical pretreatment [18]. It can produce fragmented, lower molecular weight species in high resolution mass spectra and spatial mapping while requiring minimal sample preparation steps.

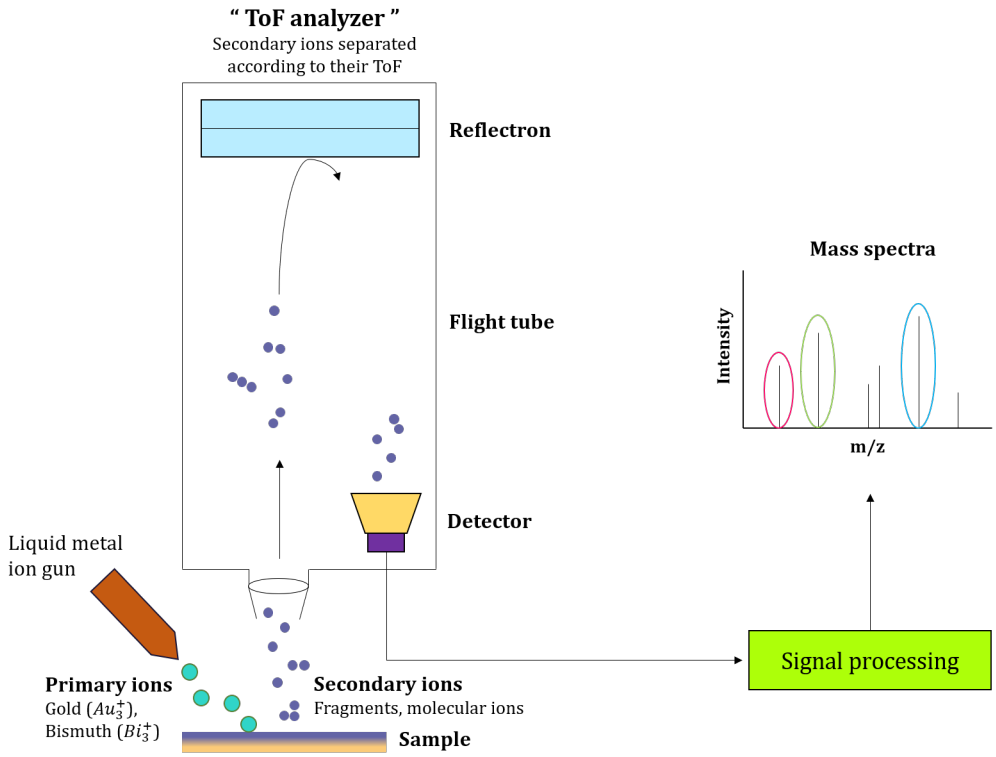

Figure 2.14: Schematic workflow of ToF-SIMS.

Generally, the ToF-SIMS consists of four parts: a primary ion source, a mass spectrometer, an ion reflectance system, and a detector. The working principle of ToF-SIMS is simple, as can be seen in figure 2.14. First, a pulsed primary ion beam from a liquid metal ion gun such as gallium (Ga^+), gold (Au_3^+), and bismuth (Bi_3^+), with an energy between 1 to 25 keV, is bombarded across the sample surface, releasing positive, negative, and neutral secondary ions from the top 1-2 nm of the sample

[19]. These secondary ions, which can be atoms or molecular ions, are accelerated by an electrostatic field and travel to the detector. The ToF-SIMS analyzer then separates the ions according to the time it takes for them to travel through the flight tube. The lighter secondary ions arrive before the heavier ones by which a mass spectrum can be recorded. The mass spectrum can be used to obtain the composition, distribution, and molecular information of the surface components [20]. Depending on the sample type being analysed, some of the ToF-SIMS settings can varied. For instance, in the case of biomass, the ToF-SIMS analyzer is configured to detect positive ions because all lignocellulosic biomass libraries are for cations [19].

With ToF-SIMS, spatially resolved images of molecules with a molecular weight of up to several thousand Daltons and with a spatial resolution of less than 100 nm can be produced [21]. Moreover, it enables parallel detection of multiple samples, excellent mass resolution, monolayer sensitivity, and the ability to record the position of a wide variety of atoms and molecules.

2.4.2 Time-of-Flight Secondary-Ion Mass Spectrometry (ToF-SIMS) on woody materials

In pulp and paper research, ToF-SIMS was first introduced in the studies of organic additives on paper surfaces [22]. Later on, the studies of chemical pulp [23] and mechanical pulp [24] where capability of ToF-SIMS were demonstrated to provide useful information about lignin structures were conducted. ToF-SIMS has been used then to analyse lignin and extractives on pulp and paper surfaces [25]–[30], using its imaging ability and analysis of molecular fragments. ToF-SIMS applications on lignocellulose include mapping of lignin, polysaccharides, extractives and inorganic components [31]–[35], evaluating pretreatment methods for hydrolysis of poplar [36] and birch [37], and studies of enzymatic and fungal degradation of wood [38].

The development of ToF-SIMS as an analytical method for the evaluation of woody materials could be used to elucidate the distribution of molecular components within different wood samples [39]. Secondary ion peaks represent characteristic of lignin, polysaccharides, and other components are shown in Table 2.1 and 2.2.

While ToF-SIMS is a promising technique for surface investigation, several limitations in currently published methods must be overcome to attain broader sample types. The main concern in the ToF-SIMS studies is directed to the possible influence of the contaminants. PDMS or polydimethylsiloxane is one of the most common organic pollutants that performs high chemical stability and is often used as a molding lubricant, plasticizer, surface modifier, antifoam agent and as a cleaning additive [40]. PDMS can easily get onto the sample surface from surrounding materials. It is important to remove the PDMS from the sample because the secondary ion yield of the PDMS is very high. To remove PDMS, n-hexane washes are effective. However, complete removal of PDMS is difficult, and solvents can also wash away some of the original chemicals from the sample. In addition, given the potential of certain

extractive compounds to form lignin-like fragment ions [41], the wood samples were extracted with solvents to reduce the likelihood of mass interference that could make the ToF-SIMS data difficult to interpret.

Table 2.1: Secondary ions reported in the literature as characteristics of lignin, carbohydrates, extractives, and inorganic compounds in wood [27], [38], [42]–[44].

Component	**Characteristic peak**	**Ion assignment**
Aromatic unit	77	$C_6H_5^+$
Aromatic unit	91	$C_7H_7^+$
Lignin		
H lignin unit	107.050	$C_7H_7O^+$
	121.029	$C_7H_5O_2^+$
	121.065	$C_8H_9O^+$
G lignin unit	137.060	$C_8H_9O_2^+$
	151.039	$C_8H_7O_3^+$
	151.076	$C_9H_{11}O_2^+$
S lignin unit	167.071	$C_9H_{11}O_3^+$
	181.050	$C_9H_9O_4^+$
	181.086	$C_{10}H_{13}O_3^+$
Carbohydrates		
Cellulose	127.040	$C_6H_7O_3^+$
	145.050	$C_6H_9O_4^+$
Xylan	115.040	$C_5H_7O_3^+$
	133.050	$C_5H_9O_4^+$
Extractives		
Fatty acids		
Myristic	211	$C_{14}H_{27}O^+$
	229	$C_{14}H_{29}O_2^+$
Pentadecanoic	225	$C_{15}H_{29}O^+$
	243	$C_{15}H_{31}O_2^+$
Palmitic	239	$C_{16}H_{31}O^+$
	257	$C_{16}H_{33}O_2^+$
Oleic	265	$C_{18}H_{34}O^+$
	283	$C_{18}H_{36}O_+$
Stearic	267	$C_{18}H_{35}O^+$
	285	$C_{18}H_{37}O_2^+$
Lignoceric	339	$C_{23}H_{47}O^+$
	351	$C_{24}H_{47}O^+$
	369	$C_{24}H_{49}O_2^+$
Pentacosanoic	355	$C_{24}H_{51}O^+$
	365	$C_{25}H_{49}O^+$
	383	$C_{25}H_{51}O_2^+$

Table 2.2: Secondary ions reported in the literature as characteristics of extractives, inorganic molecules, and contaminants (continued).

Component	Characteristic peak	Ion assignment
Extractives		
Fatty acid salts		
Calcium		
Myristate	268	$C_{14}H_{28}O_2Ca^+$
	495	$C_{28}H_{57}O_4Ca^+$
Pentadecanoate	281	$C_{15}H_{29}O_2Ca^+$
	523	$C_{30}H_{59}O_4Ca^+$
Palmitate	296	$C_{16}H_{32}O_2Ca^+$
	551	$C_{32}H_{65}O_4Ca^+$
Stearate	323	$C_{18}H_{35}O_2Ca^+$
	324	$C_{18}H_{36}O_2Ca^+$
Sodium		
Oleate	304	$C_{18}H_{33}O_2Na^+$
	305	$C_{18}H_{34}O_2Na^+$
Eicosenoate	332	$C_{20}H_{37}O_2Na^+$
	333	$C_{20}H_{38}O_2Na^+$
Lignocerate	391	$C_{24}H_{47}O_2Na^+$
	413	$C_{24}H_{48}O_2Na_2^+$
Hexadecanoate	441	$C_{26}H_{51}O_2Na_2^+$
Sterols		
Sitosterol	397	$C_{29}H_{49}^+$
	414	$C_{29}H_{50}O^+$
	415	$C_{29}H_{51}O^+$
Sitostanol	398	$C_{29}H_{50}^+$
	416	$C_{29}H_{52}O^+$
Oxo-sitosterol	411	$C_{29}H_{47}O^+$
	429	$C_{29}H_{48}O_2^+$
Inorganic		
Sodium	23	Na^+
Potassium	39	K^+
	41	K^+
Calcium	40	Ca^+

2.5 Multivariate Data Analysis

With the increasing use of computerized instrumentation, a data set can consist of thousands of input variables that contain information that is valuable for industrial and research purposes. When analyzing a large number of data sets at the same time, the number of variables and the underlying relationships between them increase significantly. As a result, reducing the number of variables while maintaining high interpretability becomes a very necessary strategy.

Multivariate data analysis includes useful methods for analyzing large data sets and principle component analysis (PCA) along with orthogonal projections to latent structures (OPLS) have proven to be extremely useful in analyzing complex sprectral data [45]. PCA, although an unsupervised method, gives an informative first look at the data set structure and relationships between groups, therefore is commonly used as a first step in multivariate data analysis. Its idea is to decrease the data complexity while maintaining as much variability as possible by calculating new variables called principal components, which represent linear combinations of the original variables and capture the greatest variation in the data set [46]. OPLS, on the other hand, is a supervised regression method that creates a better model interpretation explaining the relationship between the input variables (X) and output variables (Y). When applied to a two-class problem, this is called OPLS-DA where DA stands for discriminant analysis. OPLS-DA models the difference between groups of observations and enhances the interpretation of the class differences within a single model. Differences between sample types that are obscured by experimental variations in a PCA can thus still be identified using OPLS-DA.

3
Methodology

This chapter covers the experimental setup and analytical approach. For the experimental part, preparation and characterization of the samples were performed. As for the latter, the analysis of the samples to meet the hypothesis were done with a spectroscopic technique, TOF-SIMS, along with multivariate data analysis software SIMCA.

3.1 Paper Samples

Calendered samples (with two conditions, 100℃ and 200℃) were provided by Stora Enso.

Only the front sides of the paper were calendered at 100℃ and 200℃.

3.2 Model Materials

The reference model materials used were kraft lignin, alkali lignin, lignosulfonate (LignoStar, The Netherlands), milled wood lignin (MWL), xylan (Beechwood, Megazyme), and galactoglucomannan (GGM), cellulose nano crystals (CelluForce, Canada), microcrystalline cellulose (Avicel, USA), vanillin, furfural (Sigma-Aldrich, Germany), and extractives extracted in Soxhlet apparatus.

Most of these model materials came in powder form, except for the furfural which came in liquid form. Solutions of 0.1% w/w of each component were prepared with different solvents as shown in Table 3.1.

Table 3.1: Solvent used to dissolve each wood component.

Component	Solvent
GGM	DMSO
Xylan	DMAC
Alkali lignin	DMF
Kraft lignin	DMF
Lignosulfonate	Water
Milled wood lignin	Dioxane
Furfural	Water
Vanillin	Water

These wood components were allowed to dissolve in the solvent overnight prior to use in the next step.

3.2.1 Spin Coating

The solution from previous step was then used in the spin coating of smooth and thin films deposited onto oxidized silicon wafers which were cleaned thoroughly by exposing to a Piranha solution (1:3 v/v of H_2O_2:H_2SO_4), rinsing with Milli-Q water, and drying under nitrogen. The solution was spin-coated onto silica surfaces for 60 s at 3000 rpm 4 times each. Finally, the deposited samples were rinsed with Milli-Q water once again and dried under nitrogen. These model materials were then placed in a sterilized plastic holder before the deposition of the component was checked with AFM.

Remark: These spin-coated samples were not used as references in the analysis of calendered paper because there was a high contamination of PDMS which significantly influenced the mass spectra. Instead, the model materials were prepared in powder form onto 1x1 cm mirror-polished Si wafers using double sided tape as the attachment.

3.2.2 Soxhlet Extraction

Extractives can be extracted by organic solvents such as acetone, toluene, alcohol and water. The Soxhlet extraction was performed on wood pulp, TMP and HT-CTMP provided by Stora Enso. The two pulps were extracted using acetone as the solvent. A weight of 3 g of each pulp was prepared into a thimble and placed in a Soxhlet extractor situated above a 500 ml round-bottom flask containing 300 ml of reagent-grade acetone. The extractions were run for 16 hours in order to obtain the extractives with a composition similar as the one in calendered paper. This is done with the possibility of solvent being partly evaporated in the Soxhlet apparatus.

Remark: These extracted extractives were highly contaminated with PDMS. Therefore, the extractives used in the analysis were prepared by submerging the TMP and HT-CTMP pulp in acetone overnight. After that, all the equipment in contact with

the samples were cleaned with hexane beforehand to eliminate potential contamination. The solution were dropped onto silicon wafer until dried. These samples were then rinsed with Milli-Q water, dried under nitrogen, and placed in aluminium foil.

3.3 Analysis Equipment

3.3.1 ToF-SIMS

ToF-SIMS analysis was conducted on a ToF-SIMS V (ION-TOF, Münster, Germany), with a bismuth liquid metal ion gun as a primary ion source and a C_{60} 10 keV ion source as a sputter source. The instrument vacuum system consists of a load lock for rapid sample loading and an analysis chamber separated by the gate valve. Data were recorded in positive and negative ion modes, and high mass resolution spectra were acquired by use of a 25 keV Bi_3^+ primary ions. The Surface lab 7 software (v. 7.2; ION-TOF) was used for all spectrum. The mass spectra were internally calibrated to signals of $[C]^-$, $[CH]^-$, $[C_2]^-$, $[C_4]^-$, and $[C]^+$, and $[CH]^+$, $[CH_2]^+$, and $[CH_3]^+$ for negative and positive ion modes, respectively.

For the investigation, powder formed model materials and coated extractives were placed in the sample holder in the ToF-SIMS instrument. One to five locations on the surface of the samples were analysed.

The calendered papers processed at 100℃ and 200℃ were placed onto the sample holder and analysed on both sides. Number of locations analysed were 6 for both sides of calendered paper processed at 100℃ and 12 for both sides of the one processed at 200℃.

3.3.2 Multivariate Statistical Analysis

Principal component analysis (PCA) and orthogonal projections to latent structures discriminant analysis (OPLS-DA) were performed using multivariate software SIMCA® (SIMCA version 16.0.2, Sartorius Stedim Data Analytics AB (Umetrics), Umeå, Sweden) as MVDA methods to visualize chemical variations between calendered samples. The score plot visualizes the differences between spectra if they exist and tells if individual spectra are similar to each other or not while the loading plot indicates the variables that express this difference and shows the largest variation between spectra. The degree of similarity is mirrored within the distance between spectra in the score plot.

The fit of the PCA and OPLS-DA models can be described by the spectral variance explained by the model (R2X) and for OPLS-DA, also by the variance explained by the intensity of interest (R2Y). The Q2 value is also a measure of explained variance although it is based on cross validation and is used to estimate the predictive ability of the models. R2 and Q2 values should be in the range of 0 to 1 with Q2 value closes to 1 meaning that it is a good model. Since the reliability and prediction

properties of the models often are more important than the model fit, Q2 has a larger importance than R2 as a diagnostic tool for MVDA models.

4

Results and discussion

In this chapter, the capability of ToF-SIMS and multivariate data analysis method for identification of the wood components distributed on the surface of the calendered paper is discussed.

The visualization was first carried out with ToF-SIMS analysis of both sides of the calendered paper processed at 100℃ and 200℃. Since the data obtained were complex, multivariate data analysis was applied.

4.1 Experimental data from ToF-SIMS analysis

Through the characteristic secondary ions emitted from the paper surface, lignin, carbohydrates, extractives, and inorganic ions can be identified, and the distribution of these compounds on each paper can be determined.

4.1.1 Model materials

To facilitate the identification of components in calendered paper, each wood composition, so called model material, was analysed by ToF-SIMS spectrometry as references. Only positive secondary ion spectra were used because of low intensity observed for the characteristic peaks in the negative mode.

Approximate of 10 representative mass spectra of each lignin are displayed in Figure 4.1. As mentioned in Figure 2.5, three main patterns of methoxy substitutions on the aromatic ring in lignin are guaiacyl (G), syringyl (S), and p-hydroxyphenyl (H) units. In this case, only characteristic ions of G-type lignin were observed at m/z 137 and 151 in every samples except for alkali lignin. At high mass resolution, the peak at m/z 151 can have two peaks, the C_6-C_1 benzoyl ion and the C_6-C_2 ion, as shown in Figure 4.1a. However, in this case, it is likely that the peak at m/z 151 arises from a single component ion, the C_6-C_1 benzoyl ion, that has a C=O group at the C-7 position, because the exact mass is closer to 151.03 than 151.07. The same fragmentation was observed at m/z 165 in lignosulfonate, in which the hydroxyl (OH) group on aromatic ring was methylated to give an methoxy (OCH_3) group. Only two potential characteristic ions described lignin in alkali lignin are presented at m/z 63 and 165, as shown in Table 4.1 and 4.2 along with other potential components.

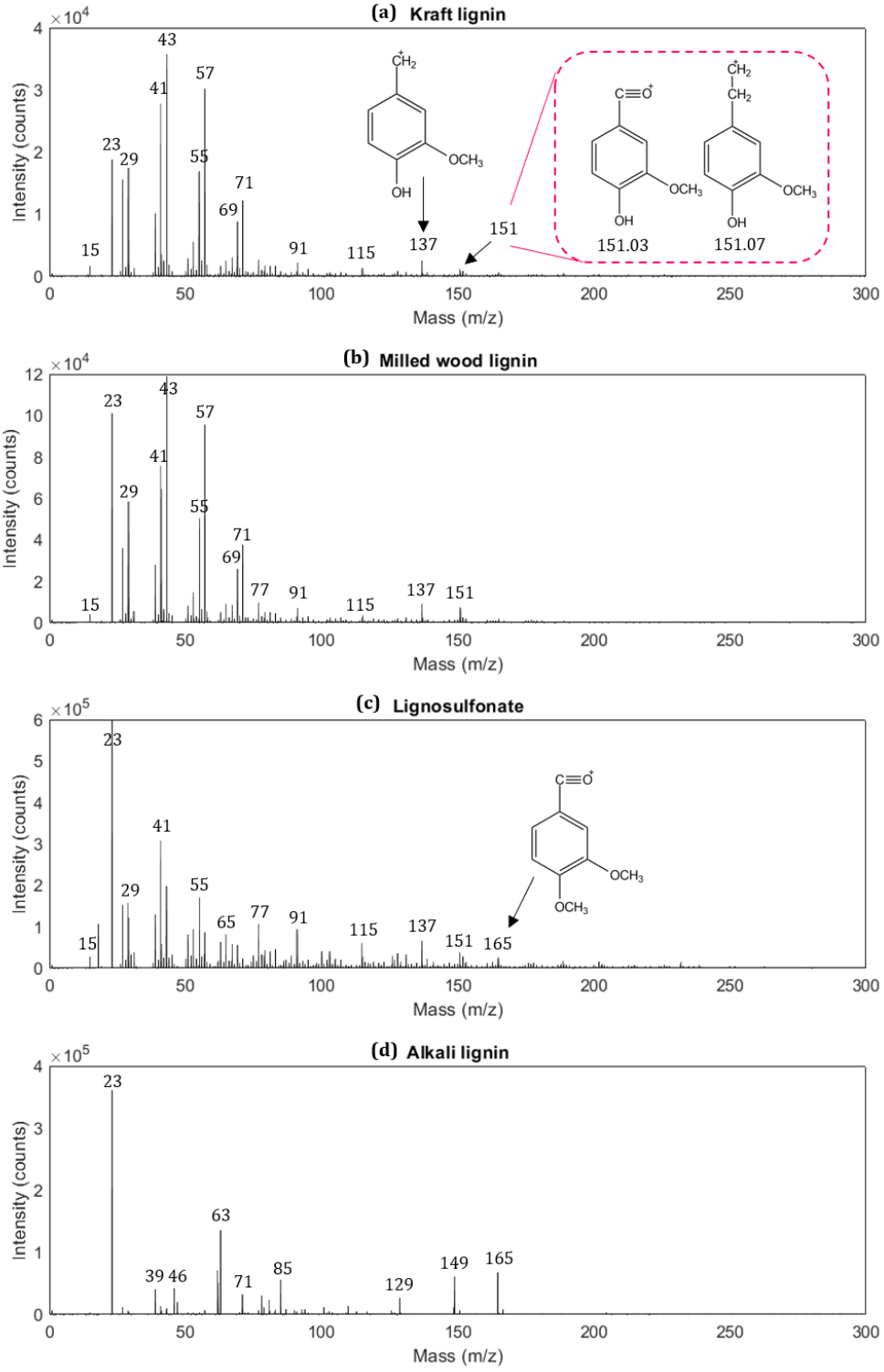

Figure 4.1: Positive ToF-SIMS spectra of lignin: (a) kraft lignin, (b) milled wood lignin, (c) lignosulfonate, and (d) alkali lignin. Exact mass of the C_6-C_1 benzoyl ion and the C_6-C_2 ion are the following: $[C_8H_7O_3]^+ = 151.0394$ and $[C_9H_{11}O_2]^+ = 151.0758$ for G-type lignin.

In agreement with literature assignments, m/z 127 and 145 peaks were characteristic of cellulose and GGM, which can be observed in (Figure 4.2a-c). The characteristic of xylan at m/z 115 and 133 can also be observed in Figure 4.2d. Other potential peaks describing polysaccharides are displayed in Table 4.1 and 4.2.

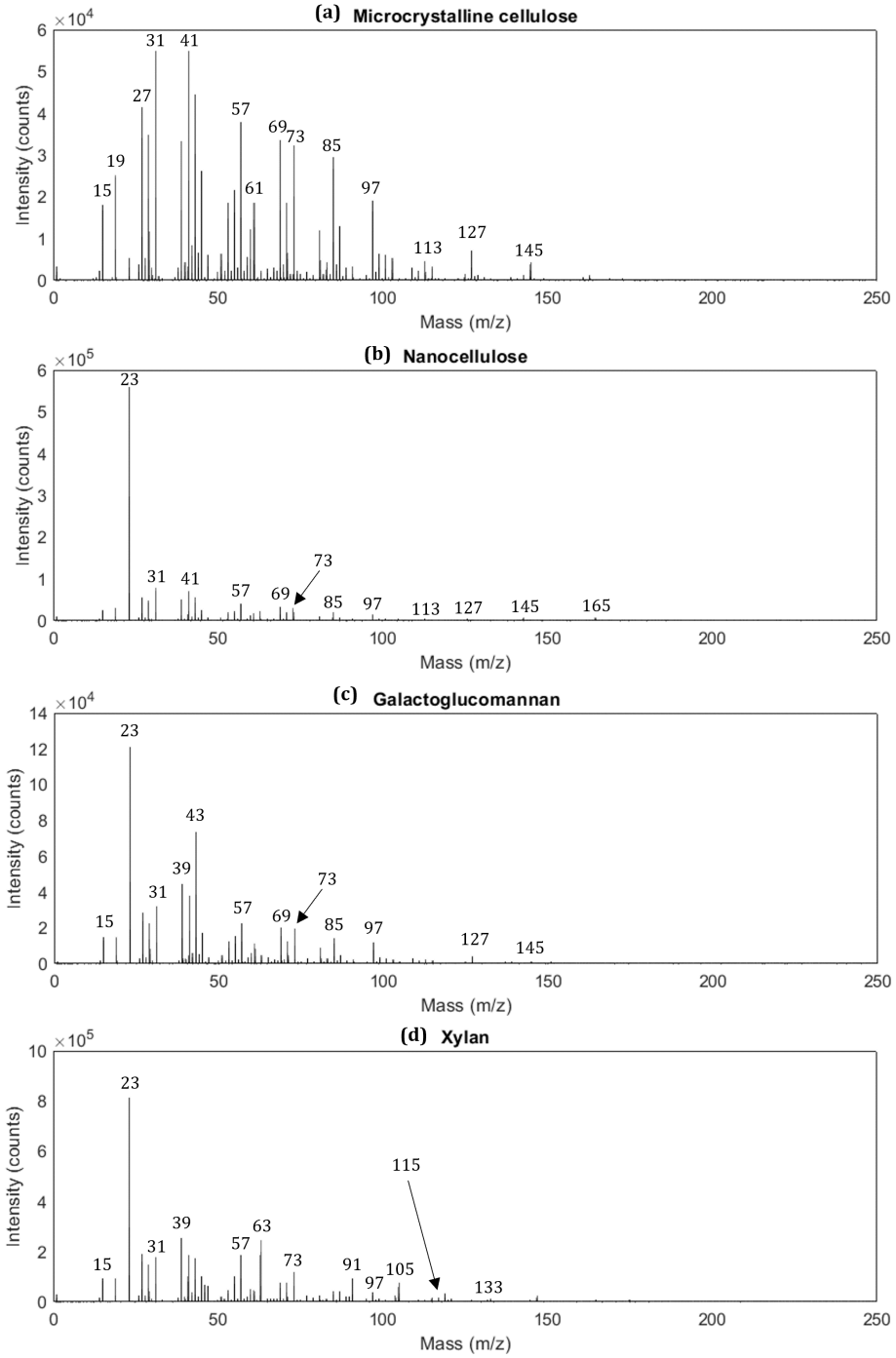

Figure 4.2: Positive ToF-SIMS spectra of polysaccharides: (a) microcrystalline cellulose, (b) nanocellulose, (c) galactoglucomannan, and (d) xylan.

Furfural and vanillin were analysed as products from hemicellulose and lignin, respectively. Extractives from TMP and HT-CTMP pulp were also analysed and displayed in Figure 4.3.

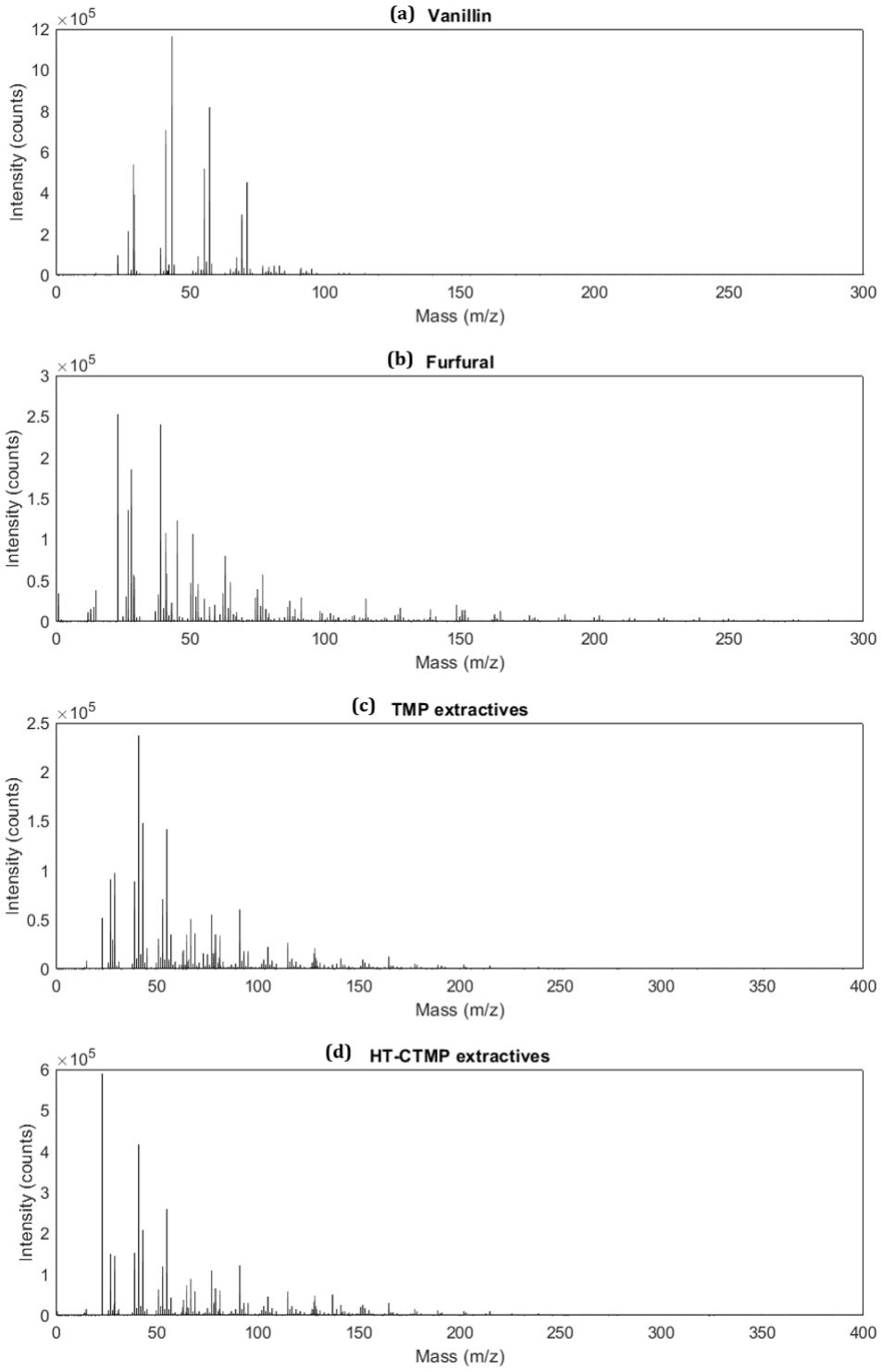

Figure 4.3: Positive ToF-SIMS spectra of (a) vanillin, (b) furfural, (c) TMP extractives, and (d) HT-CTMP extractives.

A tentative peak assignment for the qualitative chemical composition showing lignin, polysaccharides, extractives, and inorganic molecules is listed in Table 4.1 and 4.2. A complete spectra data can be seen in Appendix A.

Table 4.1: Potential characterized spectra of lignin, polysaccharides, extractives, and inorganic compounds.

Mass [m/z]	Ion assignment	Components
15	CH_3^+	Lignin, Polysaccharides
19	H_3O^+	Lignin, Polysaccharides
23	Na^+	Inorganic
27	$C_2H_3^+$	Lignin, Polysaccharides
29	CHO, $C_2H_5^+$	Lignin, Polysaccharides
31	CH_3O^+	Polysaccharides
39	K^+	Inorganic
41	$C_3H_5^+$	Polysaccharides
43	$C_3H_7^+$, $C_2H_3O^+$	Lignin, Polysaccharides
45	$C_2H_5O^+$	Polysaccharides
51	$C_4H_3^+$	Lignin
53	$C_4H_5^+$	Lignin, Polysaccharides
55	$C_4H_7^+$, $C_3H_3O^+$	Lignin, Polysaccharides
57	$C_4H_9^+$, $C_3H_5O^+$	Lignin, Polysaccharides
59	$C_2H_3O_2^+$	Polysaccharides
60	$C_2H_4O_2^+$	Polysaccharides
61	$C_2H_5O_2^+$	Polysaccharides
63	$C_5H_3^+$	Lignin
65	$C_5H_5^+$	Lignin
67	$C_5H_7^+$	Lignin
69	$C_5H_9^+$, $C_4H_5O^+$	Lignin, Polysaccharides
73	$C_3H_3O_2^+$	Polysaccharides
77	$C_6H_5^+$	Lignin
79	$C_6H_7^+$	Lignin
81	$C_6H_9^+$, $C_5H_5O^+$	Lignin, Polysaccharides
85	$C_4H_5O_2^+$	Polysaccharides
87	$C_4H_7O_2^+$	Polysaccharides
91	$C_7H_7^+$, $C_3H_7O_3^+$	Lignin, Polysaccharides
93	$C_7H_9^+$	Lignin
95	$C_7H_{11}^+$	Lignin
97	$C_5H_5O_2^+$	Polysaccharides
99	$C_5H_7O_2^+$	Polysaccharides
105	$C_8H_9^+$	Lignin
107	$C_8H_{11}^+$, $C_7H_7O^+$	Lignin
109	$C_6H_5O_2^+$	Polysaccharides
113	$C_5H_5O_3^+$	Polysaccharides
115	$C_9H_7^+$, $C_5H_7O_3^+$	Lignin, Polysaccharides
117		Extractives

Table 4.2: Potential characterized spectra of lignin, polysaccharides, extractives, and inorganic compounds.

Mass [m/z]	Ion assignment	Components
121	$C_7H_5O_2^+$, $C_8H_9O^+$	Lignin
127	$C_6H_7O_3^+$	Polysaccharides
128	$C_6H_8O_3^+$	Lignin
131	$C_5H_7O_4^+$, $C_9H_7O^+$	Lignin
137	$C_8H_9O_2^+$	Lignin
145	$C_6H_9O_4^+$	Polysaccharides
151	$C_8H_7O_3^+$, $C_5H_{11}O_5^+$	Lignin
165	$C_9H_9O_3^+$	Lignin
189	$C_{11}H_9O_3^+$	Lignin
203	$C_{11}H_9O_3^+$	Extractives
213	$C_{11}H_9O_3^+$	Extractives
215	$C_{11}H_9O_3^+$	Extractives
217	$C_{11}H_9O_3^+$	Extractives
227	$C_{11}H_9O_3^+$	Extractives
239	$C_{16}H_{32}O_2^+$	Extractives (Palmitic acid)
253	$C_{17}H_{34}O_2^+$	Extractives (Anteiso-heptadecanoic acid)
263	$C_{18}H_{32}O_2^+$	Extractives (Linoleic acid)
265	$C_{18}H_{34}O_2^+$	Extractives (Oleic acid)
267	$C_{18}H_{36}O_2^+$	Extractives (Stearic acid)
276	$C_{18}H_{34}O_2^+$	Extractives
289	$C_{18}H_{34}O_2^+$	Extractives
327	$C_{18}H_{34}O_2^+$	Extractives

Notable contributions from significant peaks mostly in lower-mass region including some higher mass are tentatively assigned in Table 4.1 and 4.2. The identified lignin peaks include the previously mentioned m/z 137 and 151 ions as well as several aromatic and benzyl ions: m/z 51, 65, 77, and 91. Some difficulty was encountered in establishing a cutoff for peaks characterizing lignin and polysaccharides in lower-mass region due to the mass overlap.

All characteristic peaks of polysaccharides corresponded to the formula $C_xH_yO_z$ except the H_3O^+ ion which results from water elimination during the fragmentation of polysaccharides in the ToF-SIMS analysis. Ions at m/z 29, 31, 57, 61, 69, 73, 85, 87, 91, 103, 115, 127, and 145 correspond to peaks previously identified in [47]. However, peaks at m/z 27, 29, 43, 53, 55, 57, 69, 81, 91, and 115 can come from either polysaccharides or lignin due to the previously mentioned mass overlap. Even so, from Figure 4.1a-c, the peak at m/z 115 shows significantly high intensity compared to the characteristic peaks of G-type lignin, m/z 137 and 151. Therefore, it might be possible that, in this study, m/z 115 represents lignin.

Here, the spectra from two wood pulp were compared to evaluate the influence of extractive compounds on ToF-SIMS spectra. Ions at m/z 239, 253, 263, 265, and 267 are identified according to literature assignments. Other peaks appeared only in

TMP and HT-CTMP pulp samples could potentially be originated from extractives. However, further study is required in order to identify all of them.

When discussing peak intensities and mass overlap, it is crucial to note that the use of different primary ion sources changes the intensity pattern of the secondary ion peaks, with gentler sources normally producing fewer fragment ions and higher molecular ion signals. Additionally, better mass resolution could theoretically distinguish where the ions originate.

4.1.2 Calendered paper

Identification of surface compounds in papers is challenging due to chemical heterogeneity of the surface, surface roughness and possible surface contamination. Therefore, six locations on each side of calendered paper processed at 100℃ and twelve for each side of the one processed at 200℃ were analyzed and the average was calculated. Each paper was being treated on one side and each side of calendered paper are illustrated in Figure 4.4 to Figure 4.7. Only the positive mode was taken for peak identification due to the lower intensity of characteristic peaks in the negative mode for paper samples.

As a result from the model materials, some peaks appeared on the surface of the calendered paper can be determined. Other peaks identify contaminant PDMS at m/z 147, 207, 221, and 281, including some inorganic peaks like sodium and potassium, were observed on every sides of the paper samples. These has significant influence on the overall mass spectra and may come from the calendering of the paper which cannot be controlled in this study.

The characteristic ions of G-type lignin, m/z 137 and 151, can be observed on the paper surfaces, as seen from Figure 4.4 to Figure 4.7, although it shows low intensity on the front side of 200℃ calendered paper which might be due to the thermal degradation of lignin. There are also many fragment ions observed in low-mass region that could potentially represent lignin and polysaccharides. These low-mass polysachharides may come from the additive during the paper production. It is possible that the starch was added to the paper to increase its strength but it is not clear how the paper was actually made in this thesis, therefore any conclusion should not be drawn.

The intensity of extractives was significantly low on the front sides, although it might be something to look out for due to a high influence of inorganic compounds. However, it seems that extractives deposited onto paper surfaces show higher intensity on the back sides of the paper for both temperatures, thus further analysis by MVDA is needed. For an overall picture, every significant peaks are listed in Table 4.3.

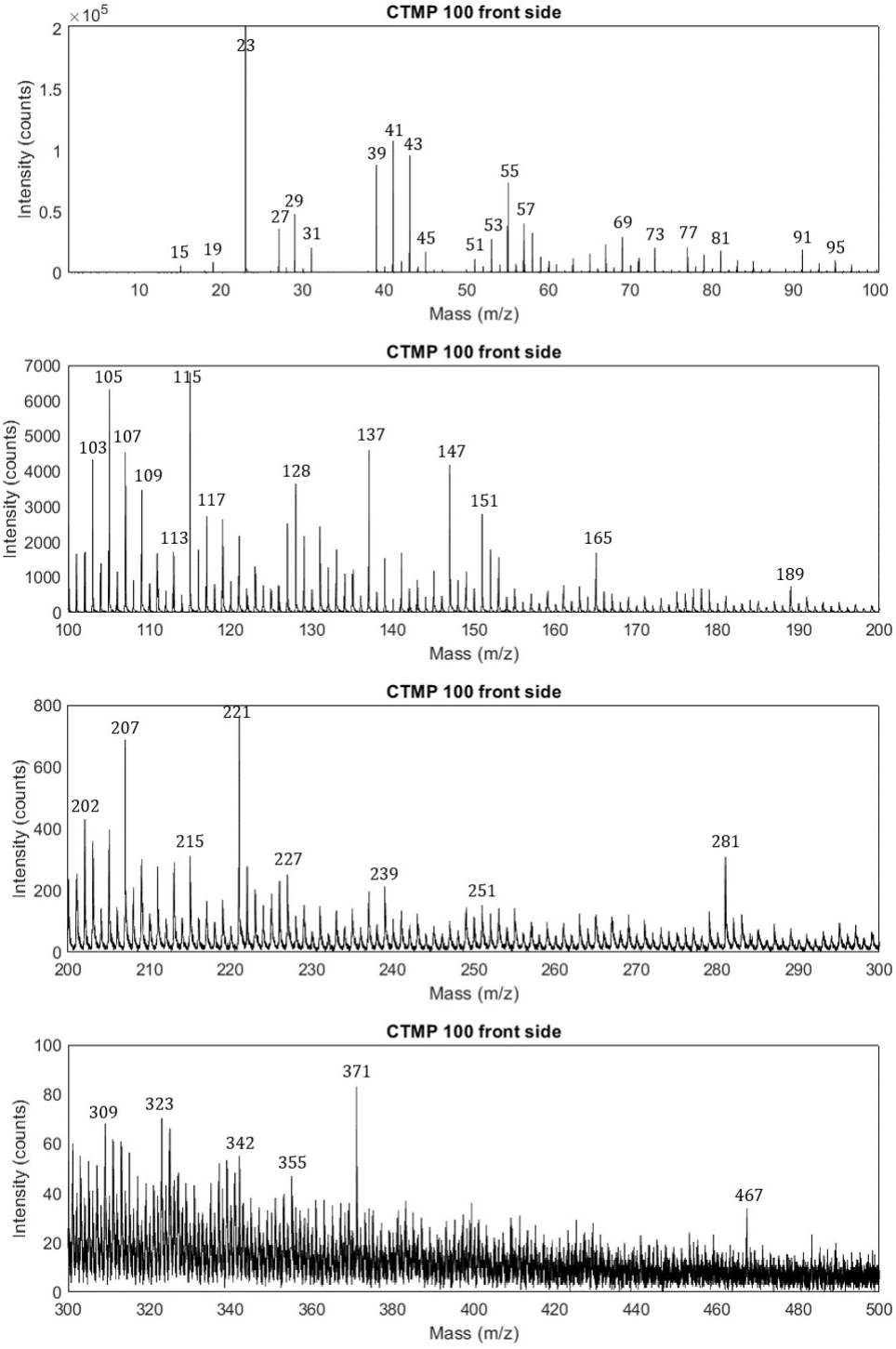

Figure 4.4: Positive ToF-SIMS spectra of 100℃ calendered paper front side.

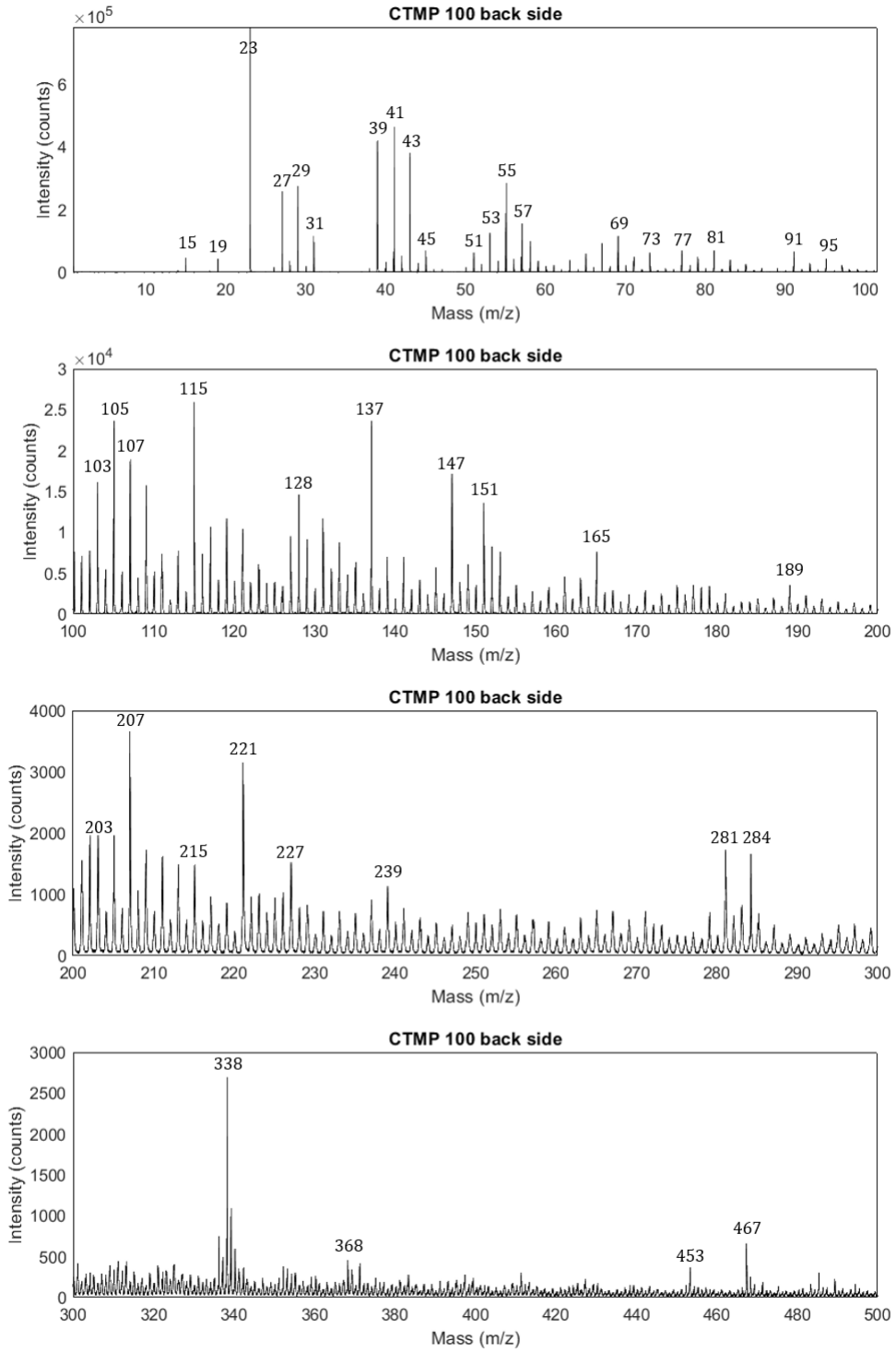

Figure 4.5: Positive ToF-SIMS spectra of 100℃ calendered paper back side.

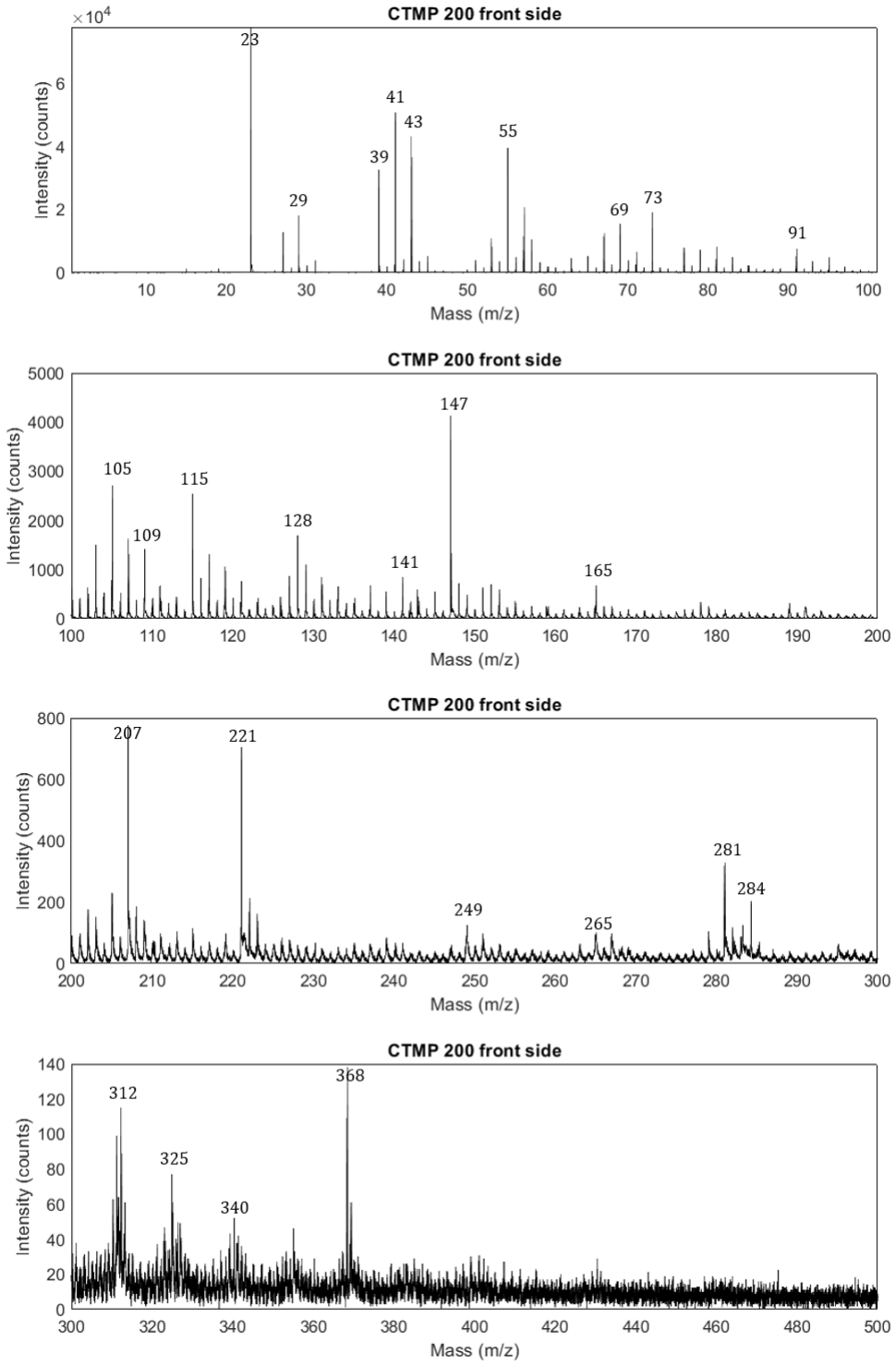

Figure 4.6: Positive ToF-SIMS spectra of 200℃ calendered paper front side.

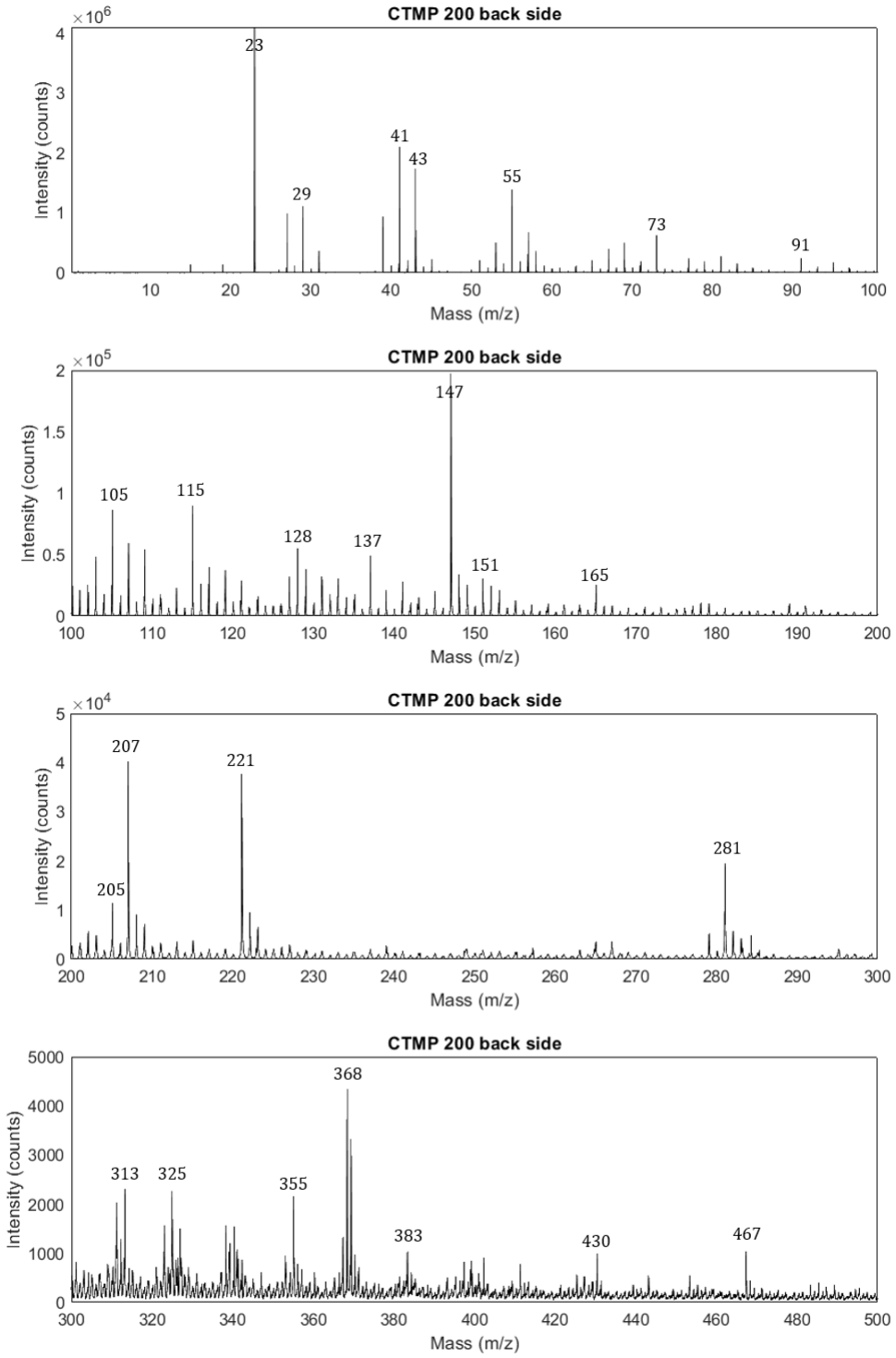

Figure 4.7: Positive ToF-SIMS spectra of 200℃ calendered paper back side.

Table 4.3: Significant peaks derived from positive ToF-SIMS spectra of calendered papers.

Peak [m/z]	**Possible component**
15.025	Lignin, Polysaccharides
19.021	Lignin, Polysaccharides
27.027	Lignin, Polysaccharides
29.044	Lignin, Polysaccharides
31.023	Polysaccharides
41.046	Polysaccharides
43.063	Lignin, Polysaccharides
45.042	Polysaccharides
51.029	Lignin
53.047	Lignin, Polysaccharides
55.065	Lignin, Polysaccharides
57.083	Lignin, Polysaccharides
59.078	Polysaccharides
65.047	Lignin
67.065	Lignin
69.085	Lignin, Polysaccharides
73.061	Polysaccharides
77.044	Lignin
79.06	Lignin
81.081	Lignin, Polysaccharides
91.063	Lignin, Polysaccharides
93.08	Lignin
95.101	Lignin
97.047	Polysaccharides
103.061	Lignin, Polysaccharides
105.076	Lignin, Polysaccharides
107.092	Lignin (H unit)
109.106	Polysaccharides
115.065	Lignin, Polysaccharides (xylan)
128.072	Lignin
137.09	Lignin (G unit)
151.072	Lignin (G unit)
165.082	Lignin
189.086	Lignin

Table 4.4: Significant peaks derived from positive ToF-SIMS spectra of calendered papers (continued).

Peak [m/z]	Possible component
203.109	Extractives
205.099	Extractives
213.09	Extractives
215.106	Extractives
227.107	Extractives
239.106	Extractives
249.071	Extractives
265.082	Extractives (Oleic)
267.105	Extractives (Stearic)
355.205	Extractives (Pentacosanoic)
368.386	Extractives (Lignoceric)
467.412	Extractives

4.2 MVDA of Variation in Mass Spectra

To identify the main contrast between four different sides of two calendered papers, PCA and OPLS-DA analyses were performed. The samples were visualized as scores from PCA projections. Figure 4.8 highlights the differences in peak patterns between samples, in this case four different groups which are front sides and back sides of both temperatures, using an axis rotation technique. The figures also show how useful MVDA of complicated ToF-SIMS spectra is to visualize the variation from chemical differences.

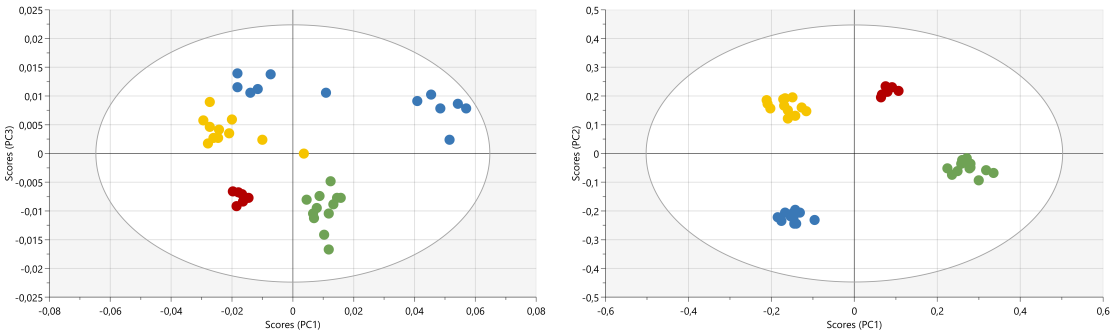

Figure 4.8: Score plots from PCA (left plot) and OPLS-DA (right plot) illustrating the difference between each side of the calendered paper. CTMP 100℃ front side (red), 100℃ back side (green), 200℃ front side (yellow), 200℃ back side (blue).

Chemical variations were further correlated to spectral variations connected to, for example, the degree of substitution properties by using OPLS-DA. The OPLS-DA grasps unique spectral features expressed in spectral loading plots which will be shown later in this chapter and gives a visualization of unique features which is similar to PCA but focused to the property in question rather than the largest spectral

variation. A good OPLS-DA model gives an accurate and simple approximation of differences between spectra to highlight differences between each side of the paper. Nevertheless, these PCA score plots indicate that all sides of the two calendered samples are chemically different from one another.

To extract more in-depth information of differences between each side of the paper, a series of OPLS-DA were performed where temperature was set to be the major factor. In Figure 4.9, the first model on the left was built with a temperature of 100℃ where the principal component 1 (PC1) divided front side (treated) and back side (untreated) from each other while PC_o1 shows the variation in the sample. In the same way, the second model on the right divided the front side and back side of 200℃ calendered paper with PC1 and illustrated the variation with PC_o1. However, due to the strong mass interferences and the influence of inorganic and contaminant PDMS on the models, it is better that peaks at m/z 73, 147, 207, 221, and 281, and mass lower than 50 be excluded from models built on nominal mass resolution spectra of calendered paper.

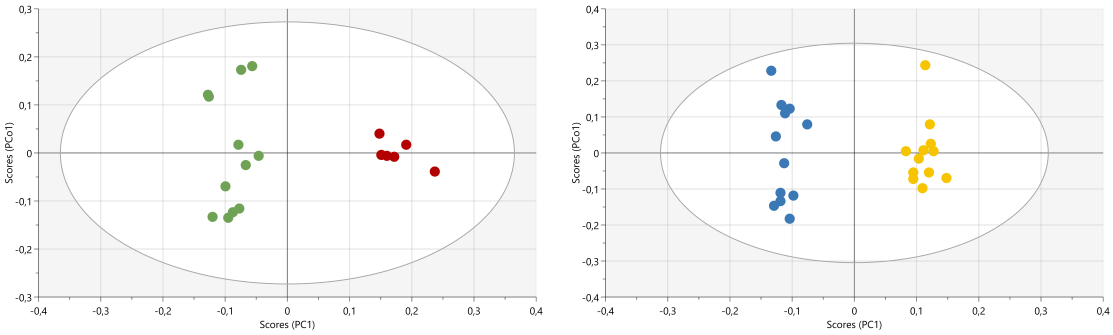

Figure 4.9: Score plots of OPLS-DA illustrating the difference between front side and back side of paper processed at 100℃ (left plot) and 200℃ (right plot), where red is 100℃ front side, green is 100℃ back side, yellow is 200℃ front side, and blue is 200℃ back side.

The loading plot of 100℃ calendered paper shown in Figure 4.10 demonstrates that there are more components spreading on the positive side of the x-axis or the front side compared to the negative side or the back side in the mass range lower than m/z 100. However, when the mass is higher than m/z 100, the majority of the components appear more on the back side. Considering higher value than absolute of -0.01 on the x-axis, two distinctive mass ions showing up more on the back side are potential fragment of lignin, m/z 79, according to the model material references and characteristic G-type lignin, m/z 137. This can be interpreted that the calendering caused the movement of the lower mass molecules or fragments, which can be a result from degradation of higher mass molecules, towards the treated side and higher mass components remain on the back side. It might also be due to the flattening of fibres which have brought all the components to the same level thus, make it more accessible for ToF-SIMS ions to fragment.

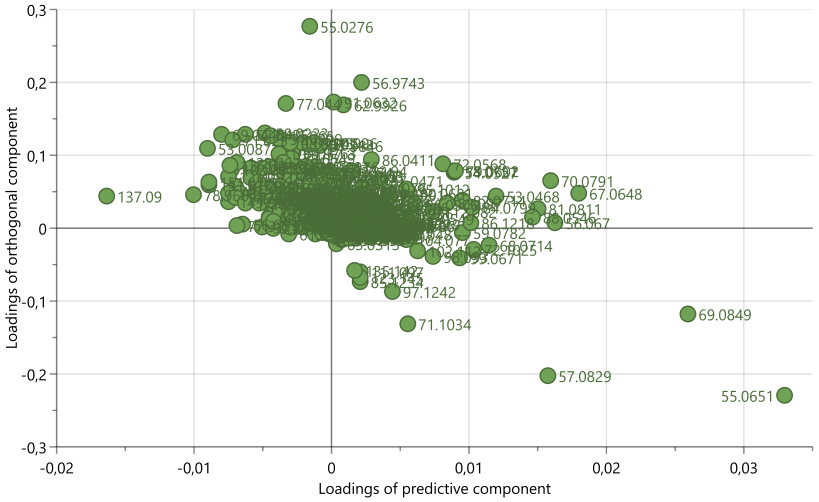

Figure 4.10: Loading plot of OPLS-DA illustrating the difference between front side (x-axis, positive) and back side (x-axis, negative) of paper processed at 100℃.

The same pattern occurred with 200℃ calendered paper shown in Figure 4.11. Considering the value higher than absolute of -0.01 on the x-axis, the components can be seen to be more distributed on the front side compared to the back side and the same two mass ions, m/z 79 and 137, distinctively appear more on the back side. However, higher temperature seems to affect the wider range of component distribution while these components seem to be more aggregated in lower temperature.

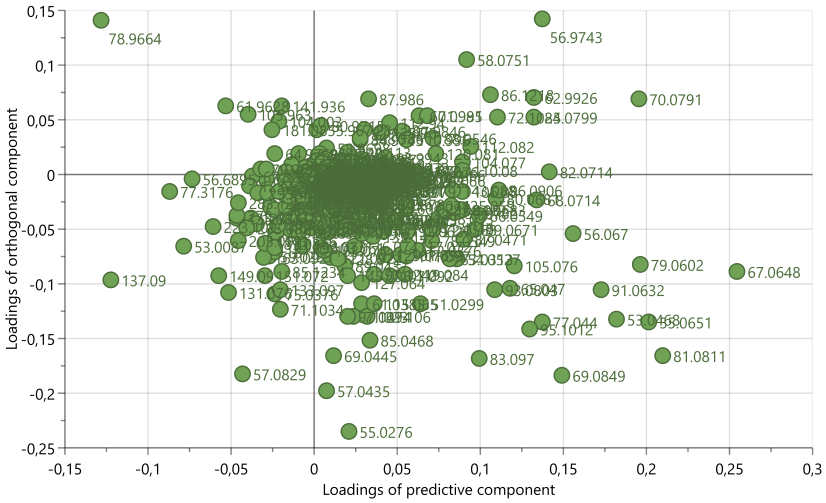

Figure 4.11: Loading plot of OPLS-DA illustrating the difference between front side (x-axis, positive) and back side (x-axis, negative) of paper processed at 200℃.

To support the assumption of the chemical differences in calendered paper, the front sides of both temperatures were compared and illustrated in score plots which can be seen in Appendix B. The model shown in Figure 4.12 was constructed with the exclusion of some peaks represent inorganic, contaminant PDMS, and mass lower than 50, the same as previously described. The peaks of interest, m/z 137 and 151,

which represent the characteristic of G-type lignin, appeared more on the front side of 100℃ calendered paper. This indicates that when temperature increases, the characteristic components might have degraded to some extent which explains the lower intensity of G-type lignin on the front side of 200℃ calendered paper.

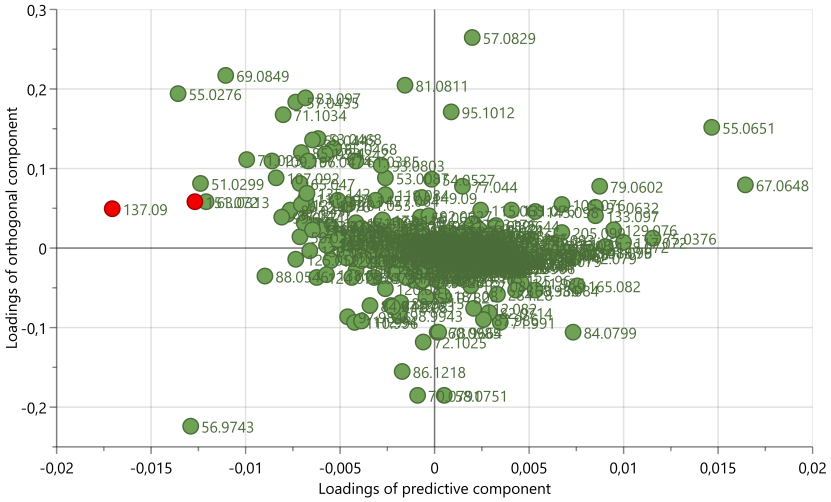

Figure 4.12: Loading plot of OPLS-DA illustrating the differences between front sides of paper processed at 100℃ (x-axis, negative) and 200℃ (x-axis, positive).

Figure 4.13 shows that the calendering might have affected the back side of the paper as well, as seen in the loading plot that m/z 137 amd 151 appeared more on the back side of 100℃ calendered paper than the back side of the 200℃ one. Therefore, it can be interpreted that higher temperature also cause the chemical degradation of characteristic components on the untreated sides.

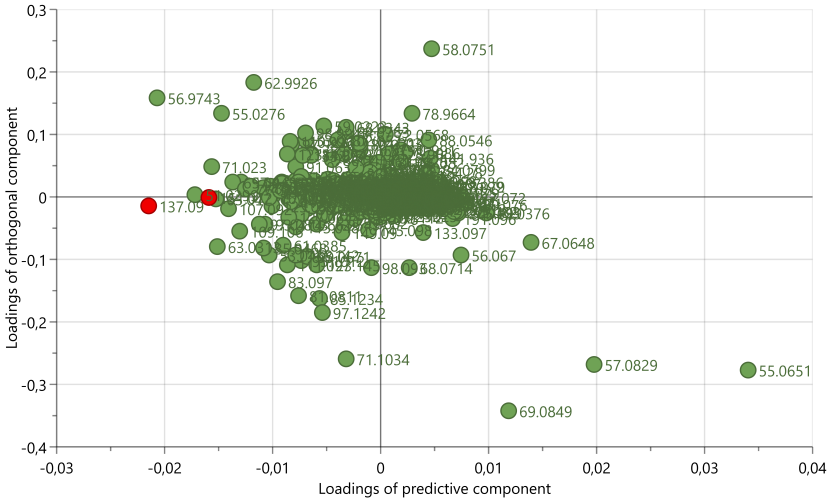

Figure 4.13: Loading plot of OPLS-DA illustrating the differences between back sides of paper processed at 100℃ (x-axis, negative) and 200℃ (x-axis, positive).

Both Figure 4.12 and Figure 4.13 support the assumption that the higher the temperature, the lower the intensity of characteristic peaks. However, it might have

to be beared in mind that these comparisons are two pieces of calendered samples processed at different temperature. Therefore, this might not be a solid conclusion.

Data for the PCA and OPLS-DA models are presented in Table 4.5. All of these models gave performance statistics, Q2 value, between 0.8 to 1 meaning that they can be described as good models.

Table 4.5: Quality data for the SIMCA models of calendered paper

Model	A	R2X	R2Y	Q2	Figure
PCA	5	0.989		0.839	4.8
OPLS-DA	3+4	0.91	0.947	0.892	4.8
OPLS-DA A	1+1	0.627	0.954	0.918	4.9
OPLS-DA B	1+3	0.781	0.98	0.943	4.9
OPLS-DA C	1+2	0.791	0.978	0.947	B.1
OPLS-DA D	1+2	0.752	0.978	0.943	B.2

A = number of PCA or OPLS-DA components. For OPLS-DA models A = 3+4 means three predictive component and four orthogonal components.

Combined, these observations imply that although almost all of the peaks were common on each side of the calendered paper, the biggest difference occurred in the amount of molecules in lower-mass region. These low-mass molecules which appeared more on the front sides can be fragments of lignin, cellulose, or hemicellulose as predicted in Table 4.3. The mass spectra higher than m/z 200 did not show any significant differences between each side of the paper. The only potential reason that chemical changes such as degradation can be presented would be due to temperature. However, it is unlikely that this is the only reaction occurred on the surface of the paper because lignin and other components tend to be stable at the calendering temperature used in this study, according to [48]. Another possibility would be cross-linking of the components as suggested in the previous study [1] which normally occur in higher temperature condition. This would lead to larger molecules or higher-mass region which cannot be seen clearly in the results.

The higher amount of extractives distributed on the back side of the paper which can be seen in Figure 4.5 and Figure 4.7 cannot be clearly observed using MVDA, as seen in the loading plots (Figure 4.10 to 4.13).

5
Conclusion

The surface of lignocellulosic material consists of many different compounds, all of which have their characteristic peaks and fragmentation patterns, thus generating their own representative spectra. This creates a challenge for ToF-SIMS spectral analysis including sensitivity loss in the high mass range. By using MVDA on such data set, it was possible to show the differences in the samples. The biggest differences between front side and back side of both calendered samples appeared in the lower-mass region with the front sides showing more fragments of lignin and polysaccharides. However, potential reactions that caused the chemical changes in the paper is likely to occur in higher-mass range which cannot be observed with ToF-SIMS analysis. Therefore, future work could be done on a more gentle method for example, GC-MS analysis, to observe the higher-mass molecules. Additionally, the morphological analysis should be performed to investigate the shininess of the calendered side of the paper which is more likely to be originated from the morphological changes rather than the chemical changes. This has on many occasions been discussed that it might be due to a shear deformation or a replication of the smooth roll surface [49].

In summary, this work was performed as a helping tool towards the expansion of ToF-SIMS secondary ions library that distinguish lignin, polysaccharides, extractives, and inorganic compounds, including the low-mass molecules in fibre products. Furthermore, the MVDA can be used to reveal the chemical differences in samples with complex spectral data, as a good complement to more time-consuming methods. However, further analysis is needed to elucidate the self-sealing mechanisms suggested in previous studies [1], [50].

Bibliography

[1] W. Svärdtröm, "Lignoseal: Additive-free sealing of paper products, Elucidation of the mechanisms", Chalmers University of Technology, Sweden, 2020.

[2] S. Suzuki, H. Shintani, S.-Y. Park, K. Saito, N. Laemsak, M. Okuma, and K. Iiyama, "Preparation of Binderless Boards from Steam Exploded Pulps of Oil Palm (Elaeis guneensis Jaxq.) Fronds and Structural Characteristics of Lignin and Wall Polysaccharides in Steam Exploded Pulps to be Discussed for Self-Bindings", *De Gruyter*, vol. 52, no. 4, pp. 417–426, Jan. 1998, ISSN: 1437-434X. DOI: 10.1515/hfsg.1998.52.4.417.

[3] Y. HaoPeng, C. ZhongRong, and G. WenLi, "Studies on bonding mechanism of dry-process binderless fibreboard. Part I. Chemical changes and effects in binderless fibreboard manufacture", *China Wood Industry*, vol. 10, no. 4, pp. 3–611, Aug. 1996.

[4] G. G. Monica Ek and G. Henriksson, Volume 1 Wood Chemistry and Wood Biotechnology. Berlin, Germany: De Gruyter, Dec. 2009, ISBN: 978-3-11-021340-9.

[5] R. J. Ross and F. P. L. U. F. Service., "Wood handbook : wood as an engineering material", *USDA Forest Service, Forest Products Laboratory, General Technical Report FPL- GTR-190, 2010: 509 p. 1 v*, vol. 190, 2010. DOI: 10.2737/FPL-GTR-190.

[6] Y. Luo, Z. Li, X. Li, X. Liu, J. Fan, J. H. Clark, and C. Hu, "The production of furfural directly from hemicellulose in lignocellulosic biomass: A review", *Catal. Today*, vol. 319, pp. 14–24, Jan. 2019, ISSN: 0920-5861. DOI: 10.1016/j.cattod.2018.06.042.

[7] J. Fahlén, "The cell wall ultrastructure of wood fibres : effects of the chemical pulp fibre line", Ph.D. dissertation, KTH, 2005.

[8] P. Fardim, J. Gustafsson, S. von Schoultz, J. Peltonen, and B. Holmbom, "Extractives on fiber surfaces investigated by XPS, ToF-SIMS and AFM", *Colloids Surf., A*, vol. 255, no. 1, pp. 91–103, Mar. 2005. DOI: 10.1016/j.colsurfa.2004.12.027.

[9] G. G. Monica Ek and G. Henriksson, Volume 2 Pulping Chemistry and Technology. Berlin, Germany: De Gruyter, Dec. 2009, ISBN: 978-3-11-021342-3. DOI: 10.1515/9783110213423.

[10] D. R. Robert, M. Bardet, G. Gellerstedt, and E. L. Lindfors, "Structural Changes in Lignin During Kraft Cooking Part 3. On the Structure of Dissolved Lignins", *J. Wood Chem. Technol.*, vol. 4, no. 3, pp. 239–263, Sep. 1984, ISSN: 0277-3813. DOI: 10.1080/02773818408070647.

[11] H. L. Hintz, "Paper: Pulping and Bleaching", in *Encyclopedia of Materials: Science and Technology*, Walthm, MA, USA: Elsevier, Jan. 2001, pp. 6707–6711, ISBN: 978-0-08-043152-9. DOI: 10.1016/B0-08-043152-6/01187-6.

[12] M. Lawoko, "Lignin polysaccharide networks in softwood and chemical pulps : characterisation, structure and reactivity", Ph.D. dissertation, KTH, 2005.

[13] P. Bajpai, "Basic Overview of Pulp and Paper Manufacturing Process", in *Green Chemistry and Sustainability in Pulp and Paper Industry*, Cham, Switzerland: Springer, 2015, pp. 11–39, ISBN: 978-3-319-18743-3. DOI: 10.1007/978-3-319-18744-0_2.

[14] D. Chaussy and D. Guérin, "Calendering of Papers and Boards: Processes and Basic Mechanisms", in *Lignocellulosic Fibers and Wood Handbook*, Chichester, England, UK: John Wiley & Sons, Ltd., Apr. 2016, pp. 493–529, ISBN: 978-1-11877372-7. DOI: 10.1002/9781118773727.ch20.

[15] R. U., "SC paper calendering technology", *Twogether special issue on finishing*, Oct. 2002.

[16] M. C. Tanzi, S. Farè, and G. Candiani, "Chapter 7 - Techniques of Analysis", in *Foundations of Biomaterials Engineering*, Cambridge, MA, USA: Academic Press, Jan. 2019, pp. 393–469, ISBN: 978-0-08-101034-1. DOI: 10.1016/B978-0-08-101034-1.00007-4.

[17] R. N. S. Sodhi, "Time-of-flight secondary ion mass spectrometry (TOF-SIMS):—versatility in chemical and imaging surface analysis", *Analyst*, vol. 129, no. 6, pp. 483–487, May 2004, ISSN: 0003-2654. DOI: 10.1039/B402607C.

[18] K. Saito, T. Kato, H. Takamori, T. Kishimoto, and K. Fukushima, "A New Analysis of the Depolymerized Fragments of Lignin Polymer Using ToF-SIMS", *Biomacromolecules*, vol. 6, no. 5, pp. 2688–2696, Sep. 2005, ISSN: 1525-7797. DOI: 10.1021/bm050147o.

[19] A. Tolbert and A. J. Ragauskas, "Advances in understanding the surface chemistry of lignocellulosic biomass via time-of-flight secondary ion mass spectrometry", *Energy Sci. Eng.*, vol. 5, no. 1, pp. 5–20, Feb. 2017, ISSN: 2050-0505. DOI: 10.1002/ese3.144.

[20] A. M. Belu, D. J. Graham, and D. G. Castner, "Time-of-flight secondary ion mass spectrometry: techniques and applications for the characterization of biomaterial surfaces", *Biomaterials*, vol. 24, no. 21, pp. 3635–3653, Sep. 2003, ISSN: 0142-9612. DOI: 10.1016/S0142-9612(03)00159-5.

[21] J. Schwieters, H.-G. Cramer, T. Heller, U. Jürgens, E. Niehuis, J. Zehnpfenning, and A. Benninghoven, "High mass resolution surface imaging with a time-of-flight secondary ion mass spectroscopy scanning microprobe", *J. Vac. Sci. Technol., A*, vol. 9, no. 6, p. 2864, Jun. 1998, ISSN: 0734-2101. DOI: 10.1116/1.577145.

[22] J. S. Brinen, "The observation and distribution of organic additives on paper surfaces using surface spectroscopic techniques", *Nord. Pulp Pap. Res. J.*, vol. 8, no. 1, pp. 123–129, Jan. 1993, ISSN: 2000-0669. DOI: 10.3183/npprj-1993-08-01-p123-129.

[23] M. Kleen, "Surface chemistry of kraft pulp fibers during TCF bleaching studies by ToF-SIMS", *Nord. Pulp Pap. Res. J.*, vol. 8, no. 1, pp. 41–44, Jan. 1993, ISSN: 2000-0669. DOI: 10.3183/npprj-1993-08-01-p123-129.

[24] ——, "ToF-SIMS as a new analytical too for studies of pulp fiber surface chemistry", *Nord. Pulp Pap. Res. J.*, vol. 8, no. 1, pp. 41–44, Jan. 1993, ISSN: 2000-0669. DOI: 10.3183/npprj-1993-08-01-p123-129.

[25] M. Kleen, "Surface lignin and extractives on hardwood RDH kraft pulp chemically characterized by ToF-SIMS", *De Gruyter*, vol. 59, no. 5, pp. 481–487, Sep. 2005, ISSN: 1437-434X. DOI: 10.1515/HF.2005.080.

[26] P. Kokkonen, P. Fardim, and B. Holmbom, "Surface distribution of extractives on TMP handsheets analyzed by ESCA, ATR-IR, ToF-SIMS and ESEM", *Nord. Pulp Pap. Res. J.*, vol. 19, no. 3, pp. 318–324, Aug. 2004, ISSN: 2000-0669. DOI: 10.3183/npprj-2004-19-03-p318-324.

[27] K. Koljonen, M. Österberg, M. Kleen, A. Fuhrmann, and P. Stenius, "Precipitation of lignin and extractives on kraft pulp: effect on surface chemistry, surface morphology and paper strength", *Cellulose*, vol. 11, no. 2, pp. 209–224, Jun. 2004, ISSN: 1572-882X. DOI: 10.1023/B:CELL.0000025424.90845.c3.

[28] P. Fardim and B. Holmbom, "ToF-SIMS imaging: a valuable chemical microscopy technique for paper and paper coatings", *Appl. Surf. Sci.*, vol. 249, no. 1, pp. 393–407, Aug. 2005, ISSN: 0169-4332. DOI: 10.1016/j.apsusc.2004.12.041.

[29] Y. Matsushita, A. Suzuki, T. Sekiguchi, K. Saito, T. Imai, and K. Fukushima, "Mapping of the cationic starch adsorbed on pulp fibers by ToF-SIMS", *Appl. Surf. Sci.*, vol. 255, no. 4, pp. 1022–1024, Dec. 2008, ISSN: 0169-4332. DOI: 10.1016/j.apsusc.2008.05.049.

[30] P. Fardim and B. Holmbom, Chemical Microscopy of Extractives on Fiber and Paper Surfaces. Dec. 2008, ISBN: 978-1-4051-5880-0. DOI: 10.1002/9781444305425.ch6.

[31] E. N. Tokareva, A. V. Pranovich, and B. R. Holmbom, "Characteristic fragment ions from lignin and polysaccharides in ToF–SIMS", *Wood Sci. Technol.*, vol. 45, no. 4, pp. 767–785, Nov. 2011, ISSN: 1432-5225. DOI: 10.1007/s00226-010-0392-9.

[32] E. N. Tokareva, P. Fardim, A. V. Pranovich, H.-P. Fagerholm, G. Daniel, and B. Holmbom, "Imaging of wood tissue by ToF-SIMS: Critical evaluation and development of sample preparation techniques", *Appl. Surf. Sci.*, vol. 253, no. 18, pp. 7569–7577, Jul. 2007, ISSN: 0169-4332. DOI: 10.1016/j.apsusc.2007.03.059.

[33] S. Jung, M. Foston, U. C. Kalluri, G. A. Tuskan, and A. J. Ragauskas, "3D Chemical Image using TOF-SIMS Revealing the Biopolymer Component Spatial and Lateral Distributions in Biomass", *Angew. Chem. Int. Ed.*, vol. 51, no. 48, pp. 12 005–12 008, Nov. 2012, ISSN: 1433-7851. DOI: 10.1002/anie.201205243.

[34] K. Saito, T. Mitsutani, T. Imai, Y. Matsushita, and K. Fukushima, "Discriminating the Indistinguishable Sapwood from Heartwood in Discolored Ancient Wood by Direct Molecular Mapping of Specific Extractives Using Time-of-Flight Secondary Ion Mass Spectrometry", *Anal. Chem.*, vol. 80, no. 5, pp. 1552–1557, Mar. 2008, ISSN: 0003-2700. DOI: 10.1021/ac7021162.

[35] K. Saito, Y. Watanabe, M. Shirakawa, Y. Matsushita, T. Imai, T. Koike, Y. Sano, R. Funada, K. Fukazawa, and K. Fukushima, "Direct mapping of mor-

phological distribution of syringyl and guaiacyl lignin in the xylem of maple by time-of-flight secondary ion mass spectrometry", *Plant J.*, vol. 69, no. 3, pp. 542–552, Feb. 2012, ISSN: 1365-313X. DOI: 10.1111/j.1365-313X.2011.04811.x.

[36] S. Jung, M. Foston, M. C. Sullards, and A. J. Ragauskas, "Surface Characterization of Dilute Acid Pretreated Populus deltoides by ToF-SIMS", *Energy Fuels*, vol. 24, no. 2, pp. 1347–1357, Feb. 2010, ISSN: 0887-0624. DOI: 10.1021/ef901062p.

[37] H.-Y. Mou, E. Orblin, K. Kruus, and P. Fardim, "Topochemical pretreatment of wood biomass to enhance enzymatic hydrolysis of polysaccharides to sugars", *Bioresour. Technol.*, vol. 142, pp. 540–545, Aug. 2013, ISSN: 0960-8524. DOI: 10.1016/j.biortech.2013.05.046.

[38] R. E. Goacher, E. A. Edwards, A. F. Yakunin, C. A. Mims, and E. R. Master, "Application of Time-of-Flight-Secondary Ion Mass Spectrometry for the Detection of Enzyme Activity on Solid Wood Substrates", *Anal. Chem.*, vol. 84, no. 10, pp. 4443–4451, May 2012, ISSN: 0003-2700. DOI: 10.1021/ac3005346.

[39] R. E. Goacher, D. Jeremic, and E. R. Master, "Expanding the Library of Secondary Ions That Distinguish Lignin and Polysaccharides in Time-of-Flight Secondary Ion Mass Spectrometry Analysis of Wood", *Anal. Chem.*, vol. 83, no. 3, pp. 804–812, Feb. 2011, ISSN: 0003-2700. DOI: 10.1021/ac1023028.

[40] D. Aoki and K. Fukushima, "Topochemical Analysis of Cell Wall Components by TOF-SIMS", *Methods Mol. Biol.*, vol. 1544, no. 249-256. 2017, ISSN: 1940-6029. DOI: 10.1007/978-1-4939-6722-3_18.

[41] R. E. Goacher, A. Y.-L. Tsai, and E. R. Master, "Towards practical time-of-flight secondary ion mass spectrometry lignocellulolytic enzyme assays", *Biotechnol. Biofuels*, vol. 6, no. 1, pp. 1–13, Dec. 2013, ISSN: 1754-6834. DOI: 10.1186/1754-6834-6-132.

[42] K. Saito, T. Kato, H. Takamori, T. Kishimoto, A. Yamamoto, and K. Fukushima, "A new analysis of the depolymerized fragments of lignin polymer in the plant cell walls using ToF-SIMS", *Appl. Surf. Sci.*, vol. 252, no. 19, pp. 6734–6737, Jul. 2006, ISSN: 0169-4332. DOI: 10.1016/j.apsusc.2006.02.163.

[43] K. Saito, T. Kato, Y. Tsuji, and K. Fukushima, "Identifying the Characteristic Secondary Ions of Lignin Polymer Using ToF-SIMS", *Biomacromolecules*, vol. 6, no. 2, pp. 678–683, Mar. 2005, ISSN: 1525-7797. DOI: 10.1021/bm049521v.

[44] P. Fardim and N. Durán, "Modification of fibre surfaces during pulping and refining as analysed by SEM, XPS and ToF-SIMS", *Colloids Surf., A*, vol. 223, no. 1, pp. 263–276, Aug. 2003, ISSN: 0927-7757. DOI: 10.1016/S0927-7757(03)00149-3.

[45] M. Hedenström, S. Wiklund-Lindström, T. Oman, F. Lu, L. Gerber, P. Schatz, B. Sundberg, and J. Ralph, "Identification of lignin and polysaccharide modifications in Populus wood by chemometric analysis of 2D NMR spectra from dissolved cell walls", *Mol. Plant*, vol. 2, no. 5, pp. 933–942, Sep. 2009, ISSN: 1674-2052. DOI: 10.1093/mp/ssp047.

[46] I. T. Jolliffe and J. Cadima, "Principal component analysis: a review and recent developments", *Philos. Trans. Royal Soc. A*, vol. 374, no. 2065, p. 20 150 202, Apr. 2016, ISSN: 1471-2962. DOI: 10.1098/rsta.2015.0202.

[47] E. S. F. Berman, K. S. Kulp, M. G. Knize, L. Wu, E. J. Nelson, D. O. Nelson, and K. J. Wu, "Distinguishing Monosaccharide Stereo- and Structural Isomers with TOF-SIMS and Multivariate Statistical Analysis", *Anal. Chem.*, vol. 78, no. 18, pp. 6497–6503, Sep. 2006, ISSN: 0003-2700. DOI: 10.1021/ac060865g.

[48] C. L. Waters, R. R. Janupala, R. G. Mallinson, and L. L. Lobban, "Staged thermal fractionation for segregation of lignin and cellulose pyrolysis products: An experimental study of residence time and temperature effects", *J. Anal. Appl. Pyrolysis*, vol. 126, pp. 380–389, Jul. 2017, ISSN: 0165-2370. DOI: 10.1016/j.jaap.2017.05.008.

[49] Volume 3 Paper Chemistry and Technology. Berlin, Germany: De Gruyter, Dec. 2009, ISBN: 978-3-11-021344-7. DOI: 10.1515/9783110213447.

[50] N. Caglar, "Fibre-fibre interactions and phase transitions of lignocellulosic substrates", Chalmers University of Technology, Sweden, 2019, available at: https://hdl.handle.net/20.500.12380/300775.

A

ToF-SIMS data

Kraft lignin	
m/z	Intensity
43,0369	34860
57,0437	29608
41,0218	26542
22,9857	18078
29,0307	17374
55,0274	16451
27,0157	15343
71,0505	11981
69,0336	8479
53,0119	5538
67,0173	2953
50,9969	2684
76,9906	2660
136,9644	2380
90,9947	2100
79,0059	1633
81,0220	1561
15,0231	1553
83,0375	1500
114,9694	1256
150,9360	1231

MWL	
m/z	Intensity
43,0427	113569
22,9892	100756
57,0536	92859
41,0269	71992
29,0334	57998
55,0356	49266
71,0625	37199
27,0178	34563
39,0109	26331
69,0449	24980
53,0190	14178
136,9875	9190
77,0020	9113
65,0110	8947
67,0275	8404
51,0033	7539
150,9584	7431
91,0089	7010
31,0100	5459
79,0185	4869
81,0349	4656
83,0521	4093
15,0233	3998
114,9892	3517
102,9973	2547

Lignosulfonate	
m/z	Intensity
22,9844	591839
41,0170	303759
43,0315	186317
55,0194	163093
27,0132	144884
29,0277	144785
76,9800	103782
18,0328	103490
90,9812	91958
53,0045	87698
57,0344	80420
50,9906	78899
64,9929	77073
136,9396	64247
62,9780	61327
114,9527	60015
67,0069	56016
69,0223	55905
83,0209	43310
78,9932	41737
102,9675	41270
81,0085	39490
100,0302	39211
150,9025	37353
31,0049	37340
127,9436	33317
130,9333	31830
125,8254	28350
164,9066	25054
188,8754	16571
231,8952	14814
162,8920	14163
201,8658	12622
160,9124	11866
177,8916	11582
175,8827	10844
202,8741	10741
176,8870	10542

Figure A.1: ToF-SIMS secondary ions represent kraft lignin, milled wood lignin, and lignosulfonate.

Alkali lignin	
m/z	Intensity
22,9847	284615
62,9203	132276
61,9083	68973
164,6948	65637
148,7317	58981
84,8640	52145
45,9389	38764
38,9361	38382
70,9142	31623
77,8784	30306
128,7862	25603
80,8589	23259
46,9486	20336
109,8038	12986
41,0097	12783
27,0085	11342
100,8302	11173
86,8853	8166
92,8614	8110
43,0430	7981
166,6853	7298
150,7208	5204
306,3801	4836

Vanillin	
m/z	Intensity
43,0319	1107818
57,0378	812508
41,0158	706223
29,0277	517714
55,0190	510810
71,0387	442402
69,0210	287769
27,0125	204869
38,9997	125455
22,9860	94974
53,0016	86728
67,0036	85949
81,0040	45356
76,9734	44118
83,0201	40555
78,9885	40466
90,9741	32730
95,0043	29479

Furfural	
m/z	Intensity
22,9865	235587
38,9528	228120
27,9696	178936
27,0180	126096
44,9650	119097
41,0278	107280
51,0063	101540
62,9995	79711
77,0082	56139
53,0211	45709
65,0155	45503
49,9981	43768
15,0230	35450
115,0001	28293
91,0158	27152
86,9856	23470
148,9486	19755
85,9772	16851
127,9993	16238
138,9842	14826
151,9817	13711
150,9638	13153
164,9824	12690
97,9696	12251
188,9643	8983

Figure A.2: ToF-SIMS secondary ions represent alkali lignin, vanillin, and furfural.

GGM	
m/z	Intensity
22,9799	119120
42,9786	71581
38,9303	42354
41,0022	36953
30,9958	31856
27,0064	27128
28,9829	22487
56,9725	21702
68,9541	19902
72,9413	18987
44,9914	16551
54,9591	14360
15,0222	13998
84,9227	13950
19,0129	13467
70,9284	12597
52,9834	11851
96,9001	11509
60,9604	11355
126,8628	3777
112,8656	2337
114,8842	1860
144,8434	1303

Xylan	
m/z	Intensity
22,9790	751894
62,9134	242726
38,9317	241749
27,0067	186901
56,9741	181150
41,0034	180640
30,9966	169592
42,9792	168243
28,9834	145229
72,9434	115907
54,9608	98941
44,9923	97288
90,8627	90666
19,0134	89490
15,0225	83485
104,8589	75213
68,9547	75209
70,9277	74192
59,9542	48901
84,9234	40872
86,8711	40470
96,9024	37078
118,8188	28106
103,8478	23654
146,7945	22933
132,8046	11291
174,8610	7874

Figure A.3: ToF-SIMS secondary ions represent galactoglucomannan and xylan.

CNC	
m/z	Intensity
22,9793	548537
30,9846	76702
40,9839	71812
42,9568	54357
26,9981	53432
38,9701	48845
28,9729	47708
56,9381	39193
68,9087	33032
19,0102	30183
72,8908	29852
44,9686	25138
15,0224	24731
54,9252	23137
62,8684	21335
52,9525	20401
84,8621	19675
70,8789	18454
60,9213	16490
96,8255	14773
59,9139	12973
41,9493	10373

CNC (cont.)	
m/z	Intensity
80,8748	9657
142,6057	8088
50,9390	8014
86,8706	7576
43,9604	6929
164,5264	6607
46,9397	6484
104,7704	4328
90,7883	4079
98,8385	3803
82,8829	3620
100,8127	3521
126,7573	3483
112,7725	3433
125,6457	2964
102,8228	2873
45,9082	2792
88,8404	2678
108,7972	2036
114,7934	1848
144,7189	1430
141,5969	1301

MCC	
m/z	Intensity
41,0061	53891
30,9985	53142
42,9828	42862
27,0082	40866
56,9782	37525
28,9849	34433
68,9606	33423
38,9916	32863
72,9491	31884
84,9318	28970
44,9951	25550
19,0139	24140
54,9644	21278
96,9109	18828
60,9664	18338
70,9359	18296
52,9877	18226
15,0228	18019
86,9441	12857
59,9587	12212
80,9412	11909
41,9740	8275
126,8756	6914
43,9871	6475
98,9236	6219
50,9736	6151
46,9708	5887
100,9000	5821
102,9139	5280
22,9810	5270
28,0138	5080
112,8776	4630
39,9970	4346
144,8581	4291
82,9513	4128

MCC (cont.)	
m/z	Intensity
69,9629	3752
26,0006	3700
85,9336	3600
90,9361	3326
114,8931	3257
88,9182	3033
66,9820	2995
37,9846	2960
108,8920	2942
29,9901	2883
55,9691	2833
64,9684	2798
67,9517	2289
51,9802	2249
110,9039	2161
73,9502	2098
53,9916	2088
62,9552	2075
57,9796	2067
49,9666	2019
97,9132	2006
76,9482	1927
81,9438	1508
83,9217	1427
124,8602	1422
78,9615	1304
74,9583	1303
142,8442	1278
162,8490	1239
94,9342	1195
128,8831	1146
32,0008	986
101,9042	839
36,9770	687
33,0106	516
48,9846	451

Figure A.4: ToF-SIMS secondary ions represent nanocellulose and microcrystalline cellulose.

TMP extractives	
m/z	Intensity
41,0320	225551
43,0475	140111
55,0431	136632
29,0354	90857
39,0152	87373
27,0196	87065
53,0259	66882
91,0253	58284
77,0152	52388
22,9883	49287
67,0379	48106
79,0310	34671
69,0541	33950
81,0483	33554
65,0206	32906
57,0579	32481
51,0104	28814
27,9714	28046
115,0117	26272
105,0357	21936
128,0113	20706
44,9685	19922
63,0049	17926
93,0424	17265
95,0589	17139
73,0313	15365
78,0217	15292
75,0031	14002
164,9999	12101
129,0197	11174
141,0128	10635
117,0272	10013
103,0177	9050
151,9971	8677
107,0528	8322
92,0295	7836
119,0459	7448
15,0229	7295
83,0646	7126
116,0169	7053
127,0036	6503
131,0390	6121
71,0700	6034
153,0010	5678
138,9978	5296
102,0107	5103
177,9941	5087
89,0086	5030
155,0245	4835
109,0688	4798
188,9842	4372
179,0070	4222
104,0251	4214
142,0192	4106
143,0320	4104

TMP extractives (cont.)	
m/z	Intensity
137,0126	4069
201,9812	3751
133,0554	3676
121,0250	3341
86,9941	3334
106,0394	3282
145,0485	3248
150,9862	3107
167,0139	3048
214,9838	2934
166,0030	2903
130,0256	2850
190,9926	2712
97,0758	2310
118,0331	2266
202,9864	2251
192,8978	2207
147,0270	2183
157,0411	2178
85,0800	2143
175,9829	2022
154,0035	1994
125,9970	1848
162,9839	1840
101,0029	1761
169,0339	1736
238,9688	1557
98,9889	1482
120,0488	1431
156,0297	1414
123,0775	1378
181,0090	1338
159,0435	1311
225,9629	1306
189,9750	1293
206,9503	1216
176,9753	1173
205,0004	1137
212,9693	1128
192,0038	1125
180,0127	1104
228,9921	1067
171,0321	995
227,9698	868
226,9572	816
251,9583	790
326,8129	744
240,9745	653
252,9645	611
262,9528	534
264,9587	502
275,9445	405
288,9514	332
324,8349	292
411,1937	252

HT-CTMP extractives	
m/z	Intensity
22,9907	547222
41,0319	402283
55,0432	244222
43,0472	192700
27,0196	147683
39,0149	140337
29,0353	136772
91,0256	115997
53,0259	113549
77,0152	103530
67,0377	87590
65,0208	70880
79,0312	65204
81,0483	59010
51,0099	58671
69,0541	57863
115,0119	57702
137,0141	49043
128,0125	45824
105,0357	44608
78,0216	29858
95,0587	29676
165,0012	29500
93,0425	28080
141,0139	25215
129,0205	23307
151,9984	22698
103,0182	21813
117,0274	21152
150,9871	18508
107,0151	16263
153,0032	15621
116,0171	15053
127,0047	14602
138,9989	13773
177,9978	13058
131,0386	12307
188,9865	11588
102,0104	11368
155,0253	10929
179,0092	10656
201,9853	10101
104,0257	9235

HT-CTMP extractives (cont.)	
m/z	Intensity
142,0204	9180
109,0692	8589
167,0148	7563
214,9874	7526
166,0040	7291
190,9959	7099
106,0394	6058
202,9892	5929
175,9855	5885
130,0262	5664
162,9852	5455
138,0157	5091
154,0064	4874
176,9869	4653
238,9726	4642
157,0426	4264
225,9682	3893
189,9813	3697
212,9723	3599
181,0076	3102
163,9774	2825
132,0090	2820
108,0205	2793
228,9939	2738
180,0135	2708
204,9993	2636
114,0045	2614
215,9892	2431
226,9651	2344
199,9682	2220
216,9985	2156
251,9624	2153
252,9752	1953
200,9629	1946
240,9795	1855
262,9562	1800
239,9744	1654
109,9981	1632
264,9667	1601
236,9559	1422
275,9496	1322
249,9482	1316
187,9616	1193
288,9531	1070

Figure A.5: ToF-SIMS secondary ions represent TMP and HT-CTMP extractives.

B

Multivariate data analysis

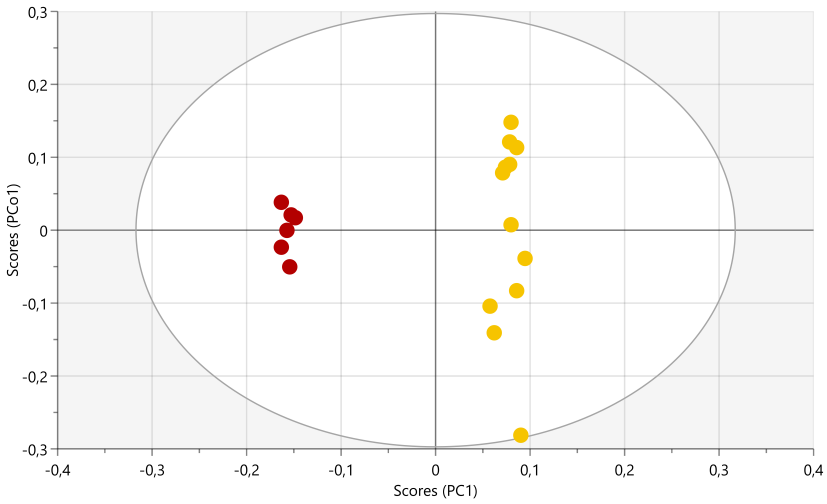

Figure B.1: Score plots of OPLS-DA illustrating the differences between front sides of two calendered papers, where red represents 100℃ and yellow represents 200℃.

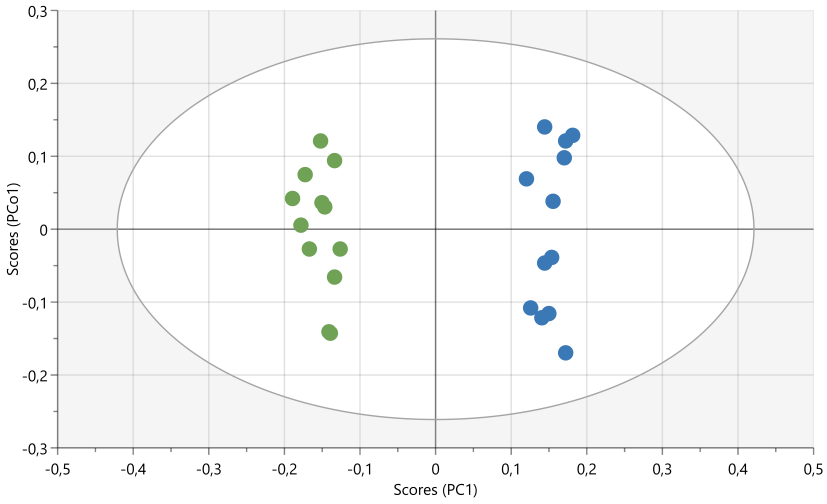

Figure B.2: Score plots of OPLS-DA illustrating the differences between back sides of two calendered papers, where green represents 100℃ and blue represents 200℃.

DEPARTMENT OF CHEMISTRY AND CHEMICAL ENGINEERING
CHALMERS UNIVERSITY OF TECHNOLOGY
Gothenburg, Sweden
www.chalmers.se

CHALMERS
UNIVERSITY OF TECHNOLOGY